J. Fluid Mech. (1982), *vol.* 118, *pp.* 411–443
Printed in Great Britain

A Fourier method for solving nonlinear water-wave problems: application to solitary-wave interactions

By J. D. FENTON AND M. M. RIENECKER
School of Mathematics, University of New South Wales,
Kensington, N.S.W., Australia 2033

(Received 8 May 1981)

A numerical method is developed for solution of the full nonlinear equations governing irrotational flow with a free surface and variable bed topography. It is applied to the unsteady motion of non-breaking water waves of arbitrary magnitude over a horizontal bed. All horizontal variation is approximated by truncated Fourier series. This and finite-difference representation of the time variation are the only necessary approximations. Although the method loses accuracy if the waves become sharp-crested at any stage, when applied to non-breaking waves the method is capable of high accuracy.

The interaction of one solitary wave overtaking another was studied using the Fourier method. Results support experimental evidence for the applicability of the Korteweg–de Vries equation to this problem since the waves during interaction are long and low. However, some deviations from the theoretical predictions were observed – the overtaking high wave grew significantly at the expense of the low wave, and the predicted phase shift was found to be only roughly described by theory. A mechanism is suggested for all such solitary-wave interactions during which the high and fast rear wave passes fluid forward to the front wave, exchanging identities while the two waves have only partly coalesced; this explains the observed forward phase shift of the high wave.

For solitary waves travelling in opposite directions, the interaction is quite different in that the amplitude of motion during interaction is large. A number of such interactions were studied using the Fourier method, and the waves after interaction were also found to be significantly modified – they were not steady waves of translation. There was a change of wave height and propagation speed, shown by the present results to be proportional to the cube of the initial wave height but not contained in third-order theoretical results. When the interaction is interpreted as a solitary wave being reflected by a wall, third-order theory is shown to provide excellent results for the maximum run-up at the wall, but to be in error in the phase change of the wave after reflection. In fact, it is shown that the spatial phase change depends strongly on the place at which it is measured because the reflected wave travels with a different speed. In view of this, it is suggested that the apparent time phase shift at the wall is the least-ambiguous measure of the change.

1. Introduction

A widely used model for the propagation of waves on water uses the approximation in which the fluid is assumed to be irrotational and incompressible, so that a velocity potential exists that satisfies Laplace's equation throughout the fluid and simple

kinematical relations on solid boundaries; both equations are linear. The nonlinearity of the water-wave propagation problem comes from the dynamic and kinematic free-surface conditions. Analytical approximations to these equations include (i) linearization, through which a host of physical problems have been solved and apparent phenomena explained, (ii) the assumption that horizontal variation is slow, giving the long-wave equations, (iii) the weakly nonlinear Schrödinger equation for deep water, and (iv) the weakly nonlinear shallow-water equations such as the Korteweg–de Vries equation and Boussinesq's equations, which have been used to study the interactions of solitary waves with some success.

As the Korteweg–de Vries (KdV) equation is used to describe the propagation and overtaking interaction of solitary waves, but is a first-order approximation only in nonlinearity and shallowness, it would be most interesting to solve the exact equations by accurate numerical means to test the applicability of the KdV equation, and to show if and where it fails to describe the interaction. Some experimental evidence (Weidman & Maxworthy 1978) suggests that it is in fact a good approximation, but no measurements of the waves *after* interaction were presented to test whether the waves emerge unscathed, as the theory predicts. For the case of two solitary waves propagating in *opposite* directions through each other, there are significant differences between experimental results (Maxworthy 1976) and theory based on Boussinesq's equations (Oikawa & Yajima 1973). Su & Mirie (1980) recast the nonlinear surface boundary conditions into a pair of equations involving the free-surface elevation and the velocity along the horizontal bottom boundary. They then determined a third-order perturbation solution to the head-on collision of two solitary waves with the result that, although the waves emerged from the collision unchanged in height, they were asymmetric and changed slowly in time. Thus some of the essential differences between approximate theory and experiment still remain. These differences need to be resolved, and perhaps the best way of doing this is to use an accurate numerical method in which many of the experimental difficulties can be avoided.

Several schemes have been proposed to solve the complete set of equations without essential analytical approximation. Chan & Street (1970) used a marker-and-cell technique to study the reflection of a solitary wave by a vertical wall. A finite spatial grid was used throughout the fluid so that the field equation was to be satisfied, by way of finite-difference approximation, at each grid point. The surface was defined by Lagrangian marker particles. It was noted that the wave after reflection was unchanged, a surprising result for an interaction during which the wave grew to a height of twice the incident wave, making the problem quite nonlinear. Brennen and Whitney (see Brennen 1971) used a Lagrangian flow description with a finite-difference mesh to study some waves generated by boundary movement. Neither of these methods seems to have been much further used. Whitney (1971), also using fluid particles to define the boundary, exploited irrotationality to use techniques of complex analysis in reducing the general problem to one that needs to be solved only on the boundary. Byatt-Smith (1971) developed a set of nonlinear integro-differential equations, and from these obtained some approximate analytical solutions, including a second-order approximation to the reflection of a solitary wave by a vertical wall. No numerical solution of his full equations has been attempted, their nonlinearity making this task rather daunting.

For water of infinite depth Longuet-Higgins & Cokelet (1976) developed a method

using boundary particles and, by exploiting irrotationality throughout the flow field, reduced the problem to one of solving a linear integral equation on the free surface as part of the time-stepping procedure. It was necessary to take great care with the finite-difference approximations, but provided this was done the method proved capable of describing even plunging breakers, as well as investigating the stability of waves on infinitely deep water. A slow numerical instability was noted, but it was suppressed by repeated smoothing. Fenton & Mills (1977) showed how that method could be applied to fluid with arbitrary solid boundaries, but were unable to produce results.

Most of the above methods depended on the use of point values to represent continuous variation and used finite-difference methods for differentiation and integration. If the flow region is large, as in the case for solitary-wave interactions, and boundary radii of curvature small, then the numerical approximations through finite differences may be rather poor. It has been shown by Fornberg & Whitham (1978) and by Abe & Inoue (1980) that spectral and pseudospectral methods, using Fourier series to represent horizontal variation, were particularly accurate and effective in solving the Korteweg–de Vries equation, and were to be preferred to finite-difference methods. Multer (1973) used Fourier methods in an attempt to solve the full nonlinear equations numerically. The free surface was defined by finitely spaced boundary particles as used in several of the finite-difference methods described above. While this is an advantage for finite-difference methods because the computational particles tend to congregate where curvatures are high, it is not an advantage for Fourier approximation (as observed by Rienecker & Fenton (1981) in Fourier approximations of steady waves). In addition, if the particles are free to move, then one of the advantages of Fourier approximation is lost, namely that the trapezoidal rule can be used for integrations with the same accuracy as the Fourier approximation. Through the use of low-order numerical integration and the accrual of rounding errors in an orthogonalization process, Multer found that the results obtained were of finite accuracy and he experienced some trouble with growing high-frequency oscillations.

In §2 the development of an alternative numerical method for solving the full nonlinear equations for wave motion on irrotational flow is described. It is based on finite-Fourier-series approximation for all spatial variation and is found to be relatively accurate and stable. In §3 its application to the interactions of solitary waves is described, for waves travelling in the same direction and also in opposite directions. A number of features of the interactions are discussed.

2. Numerical method

2.1. *Equations of motion*

A solution is sought to the equations governing the evolution of waves travelling over a layer of fluid on a horizontal bed. The more general case of an arbitrary and possibly moving bottom is considered in the appendix. All motions considered here are irrotational and two-dimensional so that a velocity potential $\phi(x, y, t)$ exists and the velocity components (u, v) are given by

$$u = \frac{\partial \phi}{\partial x}, \quad v = \frac{\partial \phi}{\partial y},$$

where x and y are respectively fixed horizontal and vertical co-ordinates with origin

on the horizontal bed. If the fluid is assumed to be incompressible, ϕ satisfies Laplace's equation throughout the fluid:

$$\frac{\partial^2\phi}{\partial x^2}+\frac{\partial^2\phi}{\partial y^2}=0. \tag{1}$$

On the free surface, defined by $y=\eta(x,t)$, the dynamic and kinematic boundary conditions must be satisfied. The dynamic condition is the pressure equation:

$$\frac{\partial\phi}{\partial t}+\frac{1}{2}\left[\left(\frac{\partial\phi}{\partial x}\right)^2+\left(\frac{\partial\phi}{\partial y}\right)^2\right]+\eta+\frac{p}{\rho}=C, \tag{2}$$

where p is the pressure on the free surface and will be assumed to be zero throughout this work, ρ is the fluid density, and C is a constant. In the above equations, and henceforth, all variables have been non-dimensionalized with respect to some depth scale h and gravitational acceleration g. The kinematic condition on $y=\eta(x,t)$ is

$$\frac{\partial\eta}{\partial t}+\frac{\partial\phi}{\partial x}\frac{\partial\eta}{\partial x}-\frac{\partial\phi}{\partial y}=0, \tag{3}$$

and the remaining kinematic condition, that no fluid pass through the horizontal bottom, is

$$\frac{\partial\phi}{\partial y}(x,0,t)=0. \tag{4}$$

It is not essential to have the origin on the bottom – it merely simplifies the equations used subsequently. In addition to the above equations, initial conditions $\phi(x,y,0)$ and $\eta(x,0)$ have to be specified.

Because of their nonlinearity there have been relatively few attempts to solve these equations without essential analytical approximations. Their essential structure is not complicated, however, for the field equation (1) and the boundary condition (4) are linear and do not contain a time derivative. The surface-boundary conditions are nonlinear, but the time derivatives in each are linear and of first order, so that, if an initial solution is known, advancing this solution in time should be a relatively simple linear process. Perhaps the most severe problem is that of approximating accurately the dependent variables $\phi(x,y,t)$ and $\eta(x,t)$ and their derivatives. In this work, variation in the horizontal direction will be approximated by Fourier series which are well known to be very accurate, provided the function approximated is sufficiently continuous. Time variation will be approximated through the use of discrete point values.

2.2. *Fourier approximation*

It is assumed that all dependent variables ϕ and η can be represented at any instant in time by Fourier series in x, throughout the region of interest. This requires that all motion be periodic in x, with some finite period L, which is referred to here as the wavelength. While this is a limitation on the general applicability of the method, there are a large number of problems in which an implied periodicity is not an important restriction. This assumption, which for the free-surface elevation may be written

$$\eta(x+L,t)=\eta(x,t),$$

is modified in the case of the velocity potential because in general it will change over

one wavelength without affecting the periodicity of the fluid motion, which only involves derivatives of ϕ. Thus

$$\phi(x+L,y,t) = \phi(x,y,t) + UL,$$

where U is some constant which can be shown to be the mean horizontal velocity of the fluid for constant y and t. Irrotationality requires U to be independent of y, and periodicity of the motion ensures that it is independent of t.

The free surface may be expressed as a finite complex Fourier series:

$$\eta(x,t) = \frac{1}{N} \sum_{j=-\frac{1}{2}N}^{\frac{1}{2}N} Y_j(t) \exp(-ijkx), \tag{5}$$

for some positive even integer N. In this expression, only half the contributions at $j = \pm \frac{1}{2}N$ are included in the summation, the $Y_j(t)$ are complex coefficients, and the wavenumber k is given by $k = 2\pi/L$. Since η is a real quantity, $Y_{-j} = Y_j^*$ (the complex conjugate of Y_j) for all j. If at any instant η is known at the N discrete points x_m, such that $kx_m = 2\pi m/N$, $m = -\frac{1}{2}N, \ldots, \frac{1}{2}N$, then the $Y_j(t)$ may be obtained by a discrete Fourier transform of the $\eta(x_m,t)$, denoted by $\mathscr{D}[\eta(m,t)]$:

$$\begin{aligned} Y_j(t) &= \sum_{m=-\frac{1}{2}N}^{\frac{1}{2}N} \eta(m,t) \exp(i2\pi mj/N) \\ &= \mathscr{D}[\eta(m,t)], \end{aligned} \tag{6}$$

where $\eta(m,t) = \eta(x_m,t)$. From (5)

$$\eta(m,t) = \frac{1}{N} \sum_j Y_j(t) \exp(-i2\pi mj/N),$$

and this is just the inverse discrete Fourier transform of $Y_j(t)$:

$$\eta(m,t) = \mathscr{D}^{-1}[Y_j(t)].$$

Again, the summation in (6) involves a factor of $\frac{1}{2}$ at the end-points $m = \pm \frac{1}{2}N$ and this is the convention assumed throughout the following work, where the limits are not shown explicitly but are to be taken as $-\frac{1}{2}N$ to $\frac{1}{2}N$. Hence the discrete transform and its inverse are essentially trapezoidal summations.

The Fourier-series approximation can be used to obtain accurate values of $\partial\eta/\partial x$ at the computational points x_m. The series (5) can be differentiated term by term with respect to x to give

$$\frac{\partial\eta}{\partial x}(x,t) = -\frac{ik}{N} \sum_j jY_j(t) \exp(-ijkx). \tag{7}$$

If $\eta(x,t)$ is sufficiently continuous the $Y_j(t)$ decay faster than any negative power of j, that is almost exponentially, and the series (7) should be a very accurate approximation to $\partial\eta/\partial x$ (despite each term being multiplied by j) provided N is large enough so that truncation of the series does not introduce unacceptable error. With $x = x_m$, (7) gives

$$\begin{aligned} \frac{\partial\eta}{\partial x}(x_m,t) &= \frac{-ik}{N} \sum_j jY_j(t) \exp(-i2\pi mj/N) \\ &= -ik\mathscr{D}^{-1}[jY_j(t)] \\ &= -ik\mathscr{D}^{-1}[j\mathscr{D}[\eta(n,t)]]. \end{aligned} \tag{8}$$

Thus the Fourier approximation can be used to give an accurate value for the derivative at any of the discrete grid points with the advantage that fast-Fourier-transform techniques can be used for computational efficiency.

$\phi(x,y,t)$ can also be represented by a Fourier series in x:

$$\phi(x,y,t) = Ux + \frac{1}{N}\sum_j \Phi(j,y,t)\exp(-ijkx), \tag{9}$$

where U is the quantity, introduced above, such that UL is the amount by which ϕ changes over one wavelength L. It is important to include this possible discontinuity in ϕ explicitly so that the $\Phi(j,y,t)$ are Fourier coefficients of a continuous function – otherwise, for a discontinuous function, the Fourier coefficients decay like $1/j$, the series would show Gibbs' phenomenon, and term-by-term differentiation would be meaningless.

If (9) is differentiated twice with respect to x, twice with respect to y, and the results substituted into Laplace's equation, (1) becomes

$$\frac{\partial^2\Phi}{\partial y^2} - j^2k^2\Phi = 0 \quad \text{for all } j,y,t.$$

The bottom boundary condition (4) is satisfied if $\partial\Phi/\partial y = 0$ for all j,t. A general solution satisfying the equations is

$$\Phi(j,y,t) = A_j(t)\frac{\cosh jky}{\cosh jkD},$$

where D is some depth, typically the mean, so that on the surface ($\eta \simeq D$) for the case of deep water the hyperbolic function ratio tends to $\exp[|j|k(\eta - D)]$, whose argument is finite and so the method can be used for all depths.

Expression (9) becomes

$$\phi(x,y,t) = Ux + \frac{1}{N}\sum_j A_j(t)\frac{\cosh jky}{\cosh jkD}\exp(-ijkx), \tag{10}$$

which satisfies Laplace's equation (1) and the bottom-boundary condition (4) identically. Expressions for ϕ_x and ϕ_y which are needed for the nonlinear surface-boundary conditions (2) and (3) are obtained by differentiating (10) term by term:

$$\phi_x(x,y,t) = U - \frac{ik}{N}\sum_j jA_j(t)\frac{\cosh jky}{\cosh jkD}\exp(-ijkx), \tag{11}$$

so that the horizontal velocity on the surface at $x = x_m$ is

$$u(m,t) = \phi_x(x_m,\eta_m,t) = U - ik\mathscr{D}^{-1}\left[jA_j(t)\frac{\cosh jk\eta(m,t)}{\cosh jkD}\right], \tag{12}$$

where $\eta_m = \eta(m,t) = \eta(x_m,t)$. Similarly, the vertical velocity at the surface may be written

$$v(m,t) = \phi_y(x_m,\eta_m,t) = k\mathscr{D}^{-1}\left[jA_j(t)\frac{\sinh jk\eta(m,t)}{\cosh jkD}\right]. \tag{13}$$

Fast-Fourier-transform techniques cannot be used to evaluate (12) and (13) because the surface elevation, which varies with m, appears in each of the terms of the Fourier inversion. The series must be evaluated formally; this can be done more quickly by exploiting the fact that $A_{-j}(t)$ is equal to $A_j^*(t)$, the complex conjugate of $A_j(t)$.

2.3. *Numerical solution of the equations*

The surface boundary conditions may be written, at the N discrete values x_m,

$$\frac{\partial \phi}{\partial t}(x_m, \eta_m, t) = C - \eta(x_m, t) - \tfrac{1}{2}[u^2(m,t) + v^2(m,t)], \tag{14}$$

$$\frac{\partial \eta}{\partial t}(x_m, t) = v(m,t) - u(m,t)\frac{\partial \eta}{\partial x}(x_m, t), \tag{15}$$

each for $m = -\frac{1}{2}N, \ldots, \frac{1}{2}N - 1$. The equations for $m = \frac{1}{2}N$ are, by periodicity, identical with the equations for $m = -\frac{1}{2}N$. If the Fourier coefficients $A_j(t)$, the surface elevations $\eta(x_m, t)$ and C are known, then all quantities on the right-hand side of these equations can be calculated using (8), (12) and (13), so that values of the time derivatives on the left-hand side are known. With the time domain represented by discrete points at intervals of Δt, so that after l intervals $t_l = l\Delta t$, finite-difference approximations are used for the time variation in (14) and (15). Of all the methods of solving systems of differential equations with initial conditions specified, one of the best compromises between accuracy and simplicity is the leapfrog method, in which centred finite differences are used. Using this, the value of η at time step $l+1$ can be found from

$$\eta(x_m, t_{l+1}) = \eta(x_m, t_{l-1}) + 2\Delta t \frac{\partial \eta}{\partial t}(x_m, t_l) + O((\Delta t)^3) \quad (m = -\tfrac{1}{2}N, \ldots, \tfrac{1}{2}N - 1).$$

Substituting (15), an explicit expression for this value of η is obtained

$$\eta(x_m, t_{l+1}) \simeq \eta(x_m, t_{l-1}) + 2\Delta t \left\{ v(m,t_l) - u(m,t_l)\frac{\partial \eta}{\partial x}(x_m, t_l) \right\} \quad (m = -\tfrac{1}{2}N, \ldots, \tfrac{1}{2}N - 1). \tag{16}$$

Advancing the rest of the solution is rather more complicated, and computationally expensive. This is because advancing the values of ϕ at points on the surface, as might be done using (14), gives information about ϕ on the arbitrary curve in space $\eta(x,t)$, from which it is not possible to obtain simply the derivatives ϕ_x and ϕ_y used in the next time step. These partial derivatives are obtained from the Fourier series (12) and (13), so that, if the updated Fourier coefficients $A_j(t_{l+1})$ can be obtained, the solution can proceed. Differentiating (10) with respect to time, and substituting $x = x_m$, $t = t_l$, and the surface elevation $y = \eta(x_m, t_l)$ gives

$$\frac{\partial \phi}{\partial t}(x_m, \eta(m,t_l), t_l) = \frac{1}{N}\sum_j \frac{\partial A_j(t_l)}{\partial t}\frac{\cosh jk\eta(m,t_l)}{\cosh jkD}\exp(-i2\pi mj/N)$$
$$(m = -\tfrac{1}{2}N, \ldots, \tfrac{1}{2}N - 1). \tag{17}$$

Values of the left-hand side are obtained from (14) at time t_l, and all quantities on the right-hand side are known at this time except the $\partial A_j(t_l)/\partial t$, for which (17) provides N linear equations (written for the N points $m = -\frac{1}{2}N, \ldots, \frac{1}{2}N - 1$). These unknowns are in fact N complex unknowns, or $2N$ real unknowns; however, in setting up the equations half of these can be eliminated by using $A_{-j}(t) = A_j^*(t)$. It is the solution of these equations which takes most computational time.

With the now known values of $\partial A_j(t_l)/\partial t$, the coefficients are stepped forward in time using the same leapfrog method as in (16):

$$A_j(t_{l+1}) = A_j(t_{l-1}) + 2\Delta t \frac{\partial A_j(t_l)}{\partial t} + O((\Delta t)^3).$$

To commence solution, initial values of $\eta(x_m, t_l)$ and $A_j(t_l)$ at $l = 0$ and 1 must be known. Obtaining these initial conditions can be a difficult procedure, and methods might vary according to the problems tackled. Discussion of the methods used in the present work will be presented in the sections where solution of specific problems is described.

2.4. *Phase errors and stability*

Apart from the choice of a finite value of N in the Fourier series representing ϕ, η and their spatial derivatives, two other factors limit the accuracy of the numerical scheme proposed above: (i) computer rounding errors, and (ii) the truncation error in the approximation of time derivatives by finite differences. The latter may be reduced by choosing a small value for the time increment Δt; however, provided reasonable accuracy can be assured, it is desirable to choose the largest-possible value of Δt so as to reduce computer time. In the numerical solution of partial differential equations the magnitude of the time increment Δt is often subject to harsh limitations to ensure stability of the scheme. In order to obtain a *guide* to an upper bound on Δt for the full nonlinear equations considered in this work, the stability of the numerical scheme for the linearized equations is investigated.

The linearized version of (1)–(4) describes the evolution of small disturbances on a uniform flow of velocity U and depth 1:

$$\frac{\partial^2 \phi}{\partial x^2} + \frac{\partial^2 \phi}{\partial y^2} = 0 \quad (-\infty < x < \infty,\ 0 < y < 1), \tag{18}$$

$$\frac{\partial \phi}{\partial y}(x, 0) = 0 \quad \text{for all } x, \tag{19}$$

$$\frac{\partial \phi}{\partial t} + U\frac{\partial \phi}{\partial x} + \eta - 1 = 0 \quad \text{on} \quad y = 1, \tag{20}$$

$$\frac{\partial \eta}{\partial t} + U\frac{\partial \eta}{\partial x} - \frac{\partial \phi}{\partial y} = 0 \quad \text{on} \quad y = 1. \tag{21}$$

A solution for ϕ satisfying (18) and (19) is

$$\phi(x, y, t) = B_1 e^{i\omega t} e^{-i\nu k x} \cosh \nu k y,$$

where k is the fundamental wavenumber, ν a positive integer such that νk is the wavenumber of this assumed solution, ω is its radian frequency, and B_1 is a constant. Similarly, if B_2 is a constant, a solution for η is

$$\eta(x, t) = 1 + B_2 e^{i(\omega t - \nu k x)}.$$

Substituting these into the linearized boundary conditions (20) and (21) gives

$$\begin{pmatrix} i\omega - i\nu k U & 1 \\ -\nu k \tanh \nu k & i\omega - i\nu k U \end{pmatrix} \begin{pmatrix} \phi(x, 1, t) \\ \eta(x, t) - 1 \end{pmatrix} = \begin{pmatrix} 0 \\ 0 \end{pmatrix},$$

and the condition that these homogeneous equations have a non-trivial solution, when the determinant of the coefficient matrix is zero, is

$$\omega = \nu k U \pm (\nu k \tanh \nu k)^{\frac{1}{2}} = \sigma(\nu k).$$

This equation is the well-known linear dispersion relation for waves travelling on a

stream of velocity U, the first term giving the Doppler contribution to the apparent frequency, as waves of wavenumber νk are convected past at speed U, the second term giving the contribution to the frequency as waves travel upstream or downstream at speed $(\tanh \nu k/\nu k)^{\frac{1}{2}}$.

If, instead of being found by direct evaluation, the time derivatives in (20) and (21) are approximated by the centred-difference scheme of §2.3, then $i\omega$ in the matrix above is replaced by $(i \sin \omega \Delta t)/\Delta t$, and the solution requires

$$\sin \omega \Delta t = \sigma(\nu k)\, \Delta t. \tag{22}$$

The numerical frequency ω is not the same as the physical frequency σ, and the physical wave lags in phase behind the numerical wave when $|\sigma \Delta t| < 1$ so that

$$\omega \simeq \sigma(1 + \tfrac{1}{6}(\sigma \Delta t)^2).$$

In the limit as $\Delta t \to 0$, $\omega = \sigma$ and there is no phase lag. This is not so when finite differences are used for spatial as well as temporal variation. Orszag (1971) has shown that the phase error is less when Fourier series are used in space than when high-order finite-difference schemes are used.

The main components of the motion, with finite amplitude but low frequency σ, will be described quite accurately by the proposed scheme of §§2.2 and 2.3. The high-frequency components will be described less accurately, but if the motion is sufficiently well-behaved the amplitudes of these components will be small.

The stability of the scheme may be investigated directly from (22). Real values of ω, corresponding to the propagation of waves without exponential growth or decay, are possible if $|\sigma(\nu k)\, \Delta t| \leqslant 1$. For positive values of σ and Δt the criterion for stability can be written

$$\Delta t \leqslant \frac{1}{\nu k |U| + (\nu k \tanh \nu k)^{\frac{1}{2}}}.$$

Examination of the denominator shows that it is a monotonically increasing function of νk, so that the most demanding criterion for stability is when ν is as large as possible, which in the present scheme is $\frac{1}{2}N$. If the fundamental wavelength L is divided into N equal steps Δx, then

$$\nu k = \tfrac{1}{2} N k = \tfrac{1}{2} N \frac{2\pi}{L} = \frac{\pi}{\Delta x},$$

and the criterion becomes

$$\Delta t \leqslant \frac{1}{\frac{\pi}{\Delta x}|U| + \left(\frac{\pi}{\Delta x} \tanh \frac{\pi}{\Delta x}\right)^{\frac{1}{2}}}. \tag{23}$$

For practical values of Δx, the $\tanh(\pi/\Delta x)$ in (23) can be approximated by unity, giving the approximate criterion

$$\Delta t \leqslant \frac{(\Delta x/\pi)^{\frac{1}{2}}}{1 + |U|(\pi/\Delta x)^{\frac{1}{2}}},$$

and the effect of a finite convective velocity U in restricting Δt is clear. Obviously it is desirable to perform calculations in a frame in which U is as small as possible, that is in a frame in which the waves travel on quiescent fluid. (However, in this frame the waves propagate at finite velocity and the time step may be governed by the truncation

error of the finite-difference approximations to the time derivatives.) In this case, $U \simeq 0$, and the approximate stability criterion becomes

$$\Delta t \leqslant (\Delta x/\pi)^{\frac{1}{2}}, \tag{24}$$

which is a particularly generous criterion compared with that obtained from finite-difference approximations to the diffusion equation, when the limiting time step is proportional to $(\Delta x)^2$, and with that obtained from Fourier approximation applied to the Korteweg–de Vries equation, when the limit is proportional to $(\Delta x)^3$ (Fornberg & Whitham 1978). In each of these methods, however, the time-stepping can be done explicitly – in the method proposed above, it is necessary to solve a matrix equation at each time step; thus the large time steps allowed by (24) are highly desirable.

The above analysis applies only to the propagation of infinitesimal waves; the question of nonlinear stability can only be answered in actual computations. This will be described in § 3 in more detail. In practice it was found that for the propagation of strongly nonlinear waves of large amplitude the linear criterion was necessary but not sufficient for stability, and most computations were done with Δt less than that allowed by the analysis. For most of the wave interactions considered the value of Δt was governed by the truncation error rather than the stability criterion. It was found that there was no slow sawtooth instability such as that described by Longuet-Higgins & Cokelet (1976). However, the method was found to suffer from a kind of nonlinear computational instability if at any stage the computations ceased to become accurate, such as when a sharp crest developed. If this occurred, the Fourier coefficients grew sufficiently for truncation of the series to be unacceptably inaccurate, leading to greater errors; the process fed on itself and quickly became unstable. Provided accuracy could be maintained, through sufficiently large values of N and sufficiently small time steps, this instability never occurred and the solution could proceed without smoothing or correction for thousands of time steps.

2.5. *Check on accuracy – evaluation of energy integrals*

Fundamental quantities that should be conserved are the mass of the fluid and the sum of the kinetic and potential energies of the motion. Evaluation of these quantities during the course of solution provides a check on the accuracy of the solution at any time. Each quantity involves integrals over the whole fluid, but can be reduced to integrals only in x. The most convenient numerical means of evaluating integrals is the trapezoidal rule, which for periodic integrands can be very accurate. In fact, it can be shown that the numerical error in evaluating an integral by using the trapezoidal rule on equispaced data at N discrete points is of the order of magnitude of the sum from $\frac{1}{2}N+1$ to ∞ of the coefficients of the Fourier series of the integrand. This is also the order of magnitude of the Fourier approximations developed in § 2.2, where the Fourier series were truncated at $\pm\frac{1}{2}N$, and all subsequent contributions ignored. Thus, it is in keeping with the accuracy of the proposed numerical method to evaluate all integrals in x by the trapezoidal rule.

Consider the fluid motion as assumed above, which is periodic in x, but of arbitrary finite amplitude. The three integrals of the motion will be obtained here in terms of quantities calculated in the course of the numerical solution.

2.5.1. *Mass of fluid.* The total mass of fluid, per unit of length normal to the flow, is

$$M = \int_{-\frac{1}{2}L}^{\frac{1}{2}L} \int_{0}^{\eta(x,t)} \rho \, dy \, dx,$$

which, because the fluid has constant density, may be written

$$M = \rho \int_{-\frac{1}{2}L}^{\frac{1}{2}L} \eta(x,t) \, dx.$$

Trapezoidal-rule evaluation of the integral gives a quantity proportional to one already used in the numerical calculations, namely the first Fourier coefficient $Y_0(t)$, as given by (6). It is convenient simply to use $Y_0(t)$, which should be constant, as a measure of mass conservation.

2.5.2. *Potential energy of fluid.* The potential energy, per unit length normal to the flow, relative to some datum h above the bottom and relative to the potential which a layer of fluid of this thickness would have is

$$\begin{aligned} V &= \int_{-\frac{1}{2}L}^{\frac{1}{2}L} \int_{1}^{\eta(x,t)} \rho(y-1) \, dy \, dx \\ &= \tfrac{1}{2}\rho \int_{-\frac{1}{2}L}^{\frac{1}{2}L} (\eta(x,t)-1)^2 \, dx \\ &\simeq \tfrac{1}{2}\rho \frac{L}{N} \sum_m (\eta(x_m,t)-1)^2, \end{aligned} \tag{25}$$

where the sum is a trapezoidal-rule sum over $-\frac{1}{2}N$ to $\frac{1}{2}N$. It should be remembered that the physical variables have been non-dimensionalized with respect to gravity, and to a depth scale h.

2.5.3. *Kinetic energy of fluid motion.* It can be shown using Green's theorem that the kinetic energy per unit length normal to the flow is

$$T = \tfrac{1}{2}\rho \oint \phi \frac{\partial \phi}{\partial n} \, ds,$$

where (s, n) are local co-ordinates, respectively tangential and outwards normal to the local boundary, ds is always taken to be positive, and the path of integration is the boundary of the computational region defined by $ABCDA$. Here AB is the horizontal bottom $y = 0$, $-\frac{1}{2}L \leqslant x \leqslant \frac{1}{2}L$; BC is the right-hand boundary $x = \frac{1}{2}L$, $0 \leqslant y \leqslant \eta(\frac{1}{2}L, t)$; DC is the free surface $y = \eta(x,t)$, $-\frac{1}{2}L \leqslant x \leqslant \frac{1}{2}L$; and AD is the left-hand boundary $x = -\frac{1}{2}L$, $0 \leqslant y \leqslant \eta(-\frac{1}{2}L, t)$. The normal velocity $\partial\phi/\partial n$ is zero on the bottom AB, so that there is no contribution to T from that boundary. This holds for any stationary solid boundary AB. The contributions from the other boundaries will be considered individually. Boundary BC gives a contribution

$$T_{BC} = \tfrac{1}{2}\rho \int_{0}^{\eta(\frac{1}{2}L,t)} \phi(\tfrac{1}{2}L, y, t) \frac{\partial \phi}{\partial x}(\tfrac{1}{2}L, y, t) \, dy,$$

and boundary AD gives

$$T_{AD} = -\tfrac{1}{2}\rho \int_{0}^{\eta(-\frac{1}{2}L,t)} \phi(-\tfrac{1}{2}L, y, t) \frac{\partial \phi}{\partial x}(-\tfrac{1}{2}L, y, t) \, dy,$$

where the negative sign occurs because $\partial/\partial n = -\partial/\partial x$ on this left-hand boundary.

Periodicity of the motion, $\eta(-\frac{1}{2}L,t)=\eta(\frac{1}{2}L,t)$, $\phi(\frac{1}{2}L,y,t)=\phi(-\frac{1}{2}L,y,t)+UL$, and $\partial\phi(\frac{1}{2}L,y,t)/\partial x=\partial\phi(-\frac{1}{2}L,y,t)/\partial x$, can be used to give

$$T_{BC}+T_{AD}=\tfrac{1}{2}\rho UL\int_0^{\eta(\frac{1}{2}L,t)}\frac{\partial\phi}{\partial x}(\tfrac{1}{2}L,y,t)\,dy. \tag{26}$$

If the expression for $\partial\phi/\partial x$ given by (11) is substituted into (26) the integral can be evaluated analytically to give

$$T_{BC}+T_{AD}=\tfrac{1}{2}\rho UL\left\{U\eta(\tfrac{1}{2}L,t)-\frac{i}{N}\sum_j A_j(t)\frac{\sinh jk\eta(\frac{1}{2}L,t)}{\cosh jkD}\right\}. \tag{27}$$

This involves only quantities already evaluated during the course of solution.

The contribution from the free surface DC is

$$T_{DC}=\tfrac{1}{2}\rho\int_D^C\phi(x,\eta(x,t),t)\frac{\partial\phi}{\partial n}(x,\eta(x,t),t)\,ds. \tag{28}$$

Along the free surface, $ds=dx(1+\eta_x^2)^{\frac{1}{2}}$, and

$$\frac{\partial\phi}{\partial n}=\frac{(\nabla\phi).(\nabla G)}{|\nabla G|},$$

where $G(x,y,t)=y-\eta(x,t)$, and ∇ is the two-dimensional gradient operator, so that

$$\frac{\partial\phi}{\partial n}=\frac{\phi_y-\phi_x\eta_x}{(1+\eta_x^2)^{\frac{1}{2}}}=\frac{\eta_t}{(1+\eta_x^2)^{\frac{1}{2}}},$$

so (28) may be written as the relatively simple integral in x:

$$T_{DC}=\tfrac{1}{2}\rho\int_{-\frac{1}{2}L}^{\frac{1}{2}L}\phi(x,\eta(x,t),t)\frac{\partial\eta}{\partial t}(x,t)\,dx \tag{29}$$

$$=\tfrac{1}{2}\rho\int_{-\frac{1}{2}L}^{\frac{1}{2}L}\{\phi(x,\eta(x,t),t)-Ux\}\frac{\partial\eta}{\partial t}(x,t)\,dx+\tfrac{1}{2}\rho U\int_{-\frac{1}{2}L}^{\frac{1}{2}L}x\frac{\partial\eta}{\partial t}(x,t)\,dx. \tag{30}$$

The integrand of (29) is not necessarily periodic but, if it is rewritten as in (30), the first integral has a periodic integrand and can be accurately evaluated with the trapezoidal rule. During the numerical time-stepping described in §2.3 it is now necessary to evaluate ϕ on the surface at each time step. This can be done efficiently at the same time that ϕ_x and ϕ_y on the surface are calculated. The $\partial\eta/\partial t$ comes from (15), evaluated during the course of the calculations. In (30) the second integral can be integrated by parts; however, to do this Fourier methods can again be implemented. Transforming the values of $\partial\eta(x_m,t)/\partial t$ obtained from (15) gives the Fourier coefficients B_j:

$$B_j=\mathscr{D}\left[\frac{\partial\eta}{\partial t}(x_m,t)\right], \tag{31}$$

and so the interpolating series becomes

$$\frac{\partial\eta}{\partial t}(x,t)=\frac{B_0}{N}+\frac{1}{N}\sum_{j\neq0}^{j}B_j\exp(-ijkx).$$

The second integral in (30) may now be evaluated to give

$$\frac{i\rho UL^2}{4\pi N}\sum_{j\neq0}^{j}(-1)^j\frac{B_j}{j}.$$

Hence, with the trapezoidal evaluation of the first integral in (30), the total kinetic energy, which incorporates (27), is given by

$$T = \tfrac{1}{2}\rho L\left\{U^2\eta(\tfrac{1}{2}L,t) - \frac{iU}{N}\sum_j A_j(t)\frac{\sinh jk\eta(\tfrac{1}{2}L,t)}{\cosh jkD}\right.$$

$$\left. + \frac{1}{N}\sum_m\left[(\phi(x_m,\eta(x_m,t),t) - Ux_m)\frac{\partial\eta}{\partial t}(x_m,t)\right] + \frac{iUL}{2\pi N}\sum_{j\neq 0}(-1)^j\frac{B_j}{j}\right\}, \quad (32)$$

where the B_j are obtained from (31).

The constancy of the total energy $T + V$ was found to be a demanding criterion, and hence helpful in program development. This was largely because the kinetic energy contains integrals of $\partial\eta/\partial t$, so that if η is accruing error this measures the *rate*, whereas the mean depth takes some time before errors are accumulated.

As a test of the accuracy of the method presented in §§2.2 and 2.3, a symmetric progressive wave of height 35 % of its mean depth and wavelength 10 times the depth was monitored for one wave period using the integral checks derived above. The initial solution was obtained from the Fourier method in Rienecker & Fenton (1981). With $N = 16$, over one wave period the total energy was conserved to within 0·003 % and total mass to within 0·002 %.

3. Interactions of solitary waves

3.1. *Application of the Fourier method*

It was not possible to model the problem of solitary-wave interactions exactly because a finite computational length L was necessary. As an approximation, waves of a long but finite length were used. The initial conditions were taken to be two waves placed adjacent to each other so that the common trough depths were the same and the fluid velocities under the troughs also the same. These waves were assumed to be of a form such that, if the other interaction wave were not present, each would progress steadily without change of form. Accurate solutions for these were obtained using the Fourier method of Rienecker & Fenton (1981), after which values of $\eta(x_m, 0)$ and $\phi(x_m, D, 0)$ for both waves combined were obtained by Fourier interpolation. Because of the implied periodicity, the problem of one wave (A) moving relative to another (B), was modelled by $...ABABABABA...$, an infinite train of AB interactions. The waves were chosen long enough so that this did not affect their interaction, as verified by preliminary numerical tests; that each wave closely approximated a solitary wave was justified by comparing phase speeds and integral quantities with those given by Fenton (1972).

The time-stepping method needs two sets of initial conditions, at time zero and at one step Δt later. These were obtained by allowing each wave of the above initial solution to travel a distance $c\Delta t$, where c is its wavespeed in a frame of reference such that the fluid velocity under the common trough is zero. Then, by assuming each wave to be still unaffected by the other, the $\eta(x_m, \Delta t)$ and $\phi(x_m, D, \Delta t)$ were obtained by Fourier interpolation. The time-stepping could then be started.

It should be noted that the case of long-wave interactions is a particularly demanding test of the Fourier method. This is because the Fourier coefficients for long waves show a much wider spectrum than for shorter waves. A long wave is essentially a single hump on otherwise undisturbed fluid: to model this by Fourier series requires many more terms in the series than a wave in deep water, which more closely resembles a sine wave. Accordingly, for long waves larger values of N are necessary, and because the solution of the set of linear equations at each step involves a process proportional to N^3, much more computer effort is necessary.

3.2. *One solitary wave overtaking another*

3.2.1. *Computational details.* In this case the waves move slowly relative to one another, the interaction time is long, and so is the computational time necessary to simulate the physical situation. After some trial and error it was found that $N = 64$ was necessary to solve this problem accurately, and a single time step took 5·3 s on the Cyber 171 computer at the University of New South Wales. A typical solitary-wave-interaction problem was estimated to take some 8 h of computer time, which was considered too long to examine a number of different interactions. One interaction only was studied, the results of which justify the application of approximate theory, rendering further accurate numerical studies rather superfluous.

The two waves used were a wave of height 30 % of its mean depth and a wavelength of about 15 times the depth joined to a wave of height 10 % of its mean depth and a wavelength of about 20 times the depth. As described in §3.1, the waves were joined together at the trough. The length scale used in this paper is the depth h under this common trough of the two waves, corresponding to the undisturbed depth of water far from a solitary wave. The heights of the two 'solitary' waves using this length scale were

$$\text{high wave height} = \epsilon_A = 0{\cdot}3252,$$

$$\text{low wave height} = \epsilon_B = 0{\cdot}1035,$$

$$\text{with wave-height ratio} = \epsilon_A/\epsilon_B = 3{\cdot}142,$$

so that solutions of the weakly nonlinear Korteweg–de Vries equation, as obtained by Hirota (1971), predict a class (c) interaction, that is at the centre of the interaction there is only one crest (see Weidman & Maxworthy (1978) for a description of the three classes (a), (b) and (c)). As described above, $N = 64$ was used, while the computational wavelength $L/h = 37{\cdot}4$, so that $\Delta x/h = 0{\cdot}584$ – about half the depth, and a rather coarse grid spacing by finite-difference standards. The dimensionless time step Δt ($= \Delta t(g/h)^{\frac{1}{2}}$ in dimensional terms) was 0·052, about $\frac{1}{20}$ of the time taken for a solitary wave to traverse a distance equal to the water depth. Choice of such a small time step was dictated by considerations of accuracy rather than stability. The total number of time steps taken, for the interaction and for the waves to be far enough apart afterwards for the interaction to be considered complete was 5700, in which time the high crest travelled a total distance of about 340, that is about 9 times through the computational wavelength.

3.2.2. *Description of the interaction.* The interaction is shown in figures 1 and 2. In figure 1 each continuous curve shows the surface at an instant in time, the next curve behind it corresponds to another later time. The figure is plotted from the point of view of an observer moving at the initial speed of the lower wave. Initially, neither of the separate humps senses the presence of the other; however, they gradually merge

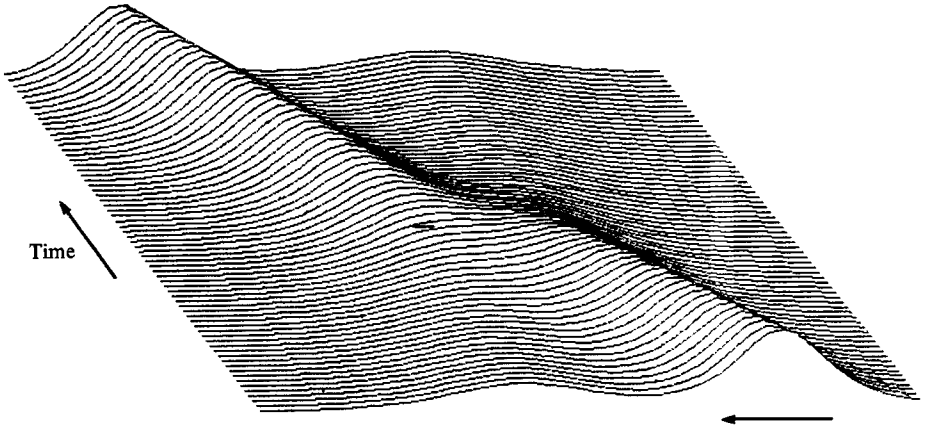

FIGURE 1. Overtaking solitary-wave interaction as viewed by an observer travelling at the initial speed of the lower wave. Initial wave heights are 0·3252 and 0·1035 of the undisturbed depth.

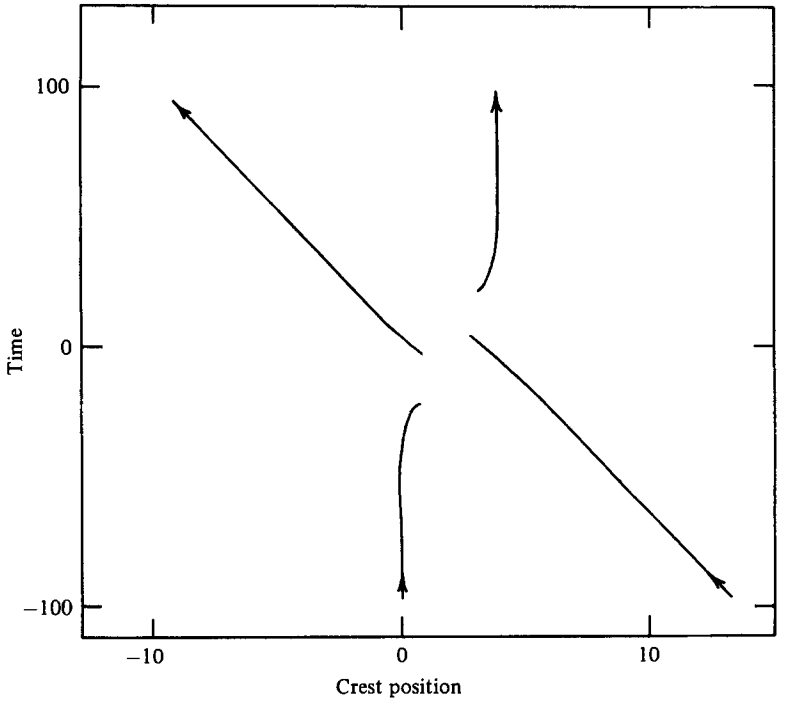

FIGURE 2. Crest trajectories of the waves, relative to an observer initially located at the crest of the slow wave and continuing to move with that crest speed even after interaction. The disappearance of that crest, its subsequent reappearance in the same position, this time as a fast crest, and the apparent phase shift of the crests can be identified.

until at the centre of the interaction the wave is a single mount whose crest region looks quite flat. Close examination of the figure shows that just before (and just after) the centre of the interaction there is only one *crest* (local maximum of elevation), but that, at the interaction centre, there is a slight trough between two crests. It is clear that, unlike predictions from the Korteweg–de Vries equation, this interaction is

actually of type (*b*). In this case the higher wave passes its substance to the other one so that two distinct wave masses can always be identified, even though there is actually only one *crest* at certain stages of the interaction. Figure 2 shows the existence and position of crests at different times, with position plotted horizontally (relative to a moving co-ordinate system in which the original lower wave is stationary), and time plotted vertically. At any time, intersection of the curves with a horizontal line gives the position of crests. The interaction will now be described in some detail, as illustrated by these figures.

It is not until the crests are close together that any significant interaction occurs. When this occurs fluid flows from the high wave to the intermediate trough and into the other lower wave while their relative positions are essentially maintained. At a certain stage the trough has been filled so that, while one *crest* has disappeared, clearly there is an identifiable mass of liquid roughly where that crest has been. The higher crest continues to drop as fluid is extracted from it and passed forward until enough has changed position that a crest reappears where the lower crest was. Now there are two crests separated by a finite distance, but with one continuing to grow at the expense of the other until the system is symmetrical with two equal crests and a barely discernible trough between them. Whereas the initial crest elevations of the two waves were 1·3252 and 1·1035, both crests (separated by distance 2·946 – three times the undisturbed depth) now have a height of only 1·2096, while the trough has elevation 1·2053. When plotted on Weidman & Maxworthy's figures for the geometry of the waves at the centre of interaction, these numbers show consistent agreement with the experimental results. An important feature of the interaction is that the maximum elevation at the interaction centre is considerably less than that of the highest incident wave, and the crests are widely separated so that the interaction occurs with relatively low heights and accordingly relatively weak nonlinearities and interactions so that it should be capable of description by the Korteweg–de Vries equation. A qualitative difference between the solutions of that equation and the present results is in the type of interaction (types (*c*) and (*b*) respectively). If, however, the trough shown in figure 1 contained *slightly* more fluid, then instead of crest–trough–crest, a single crest would be seen and the interaction would be classified as being of type (*c*). It does seem that there is no important difference between the interactions of types (*a*), (*b*) and (*c*), which are illustrated in Weidman & Maxworthy (1978). In each case the faster rear wave passes its form to the slower front wave by a similar process. The classification into different types of interaction, based on phenomena of crest behaviour, seems to have little to do with the real nature of the interaction.

3.2.3. *Post-interaction behaviour.* Events after the waves reach equal height are very nearly the reverse of what happened before (while KdV theory predicts precisely the reverse). The forward wave continues to grow at the expense of the rear wave until it acquires substantially the characteristics of the initial rear wave; it is then higher and faster, and accordingly moves off. The rear wave temporarily loses its crest just as the front wave momentarily lost its crest, until the waves are sufficiently separate, after which the rear wave propagates independently as the small and slow wave. After interaction the crest elevations are $1{\cdot}3288 \pm 1$ and $1{\cdot}1017 \pm 2$. Thus the high wave has grown by 0·0036 (1·1 % of the wave height), while the low wave has decreased by 0·0018 (1·7 %). These small deviations from the theory, which predicts no change, show that the front wave is even more parasitic in its effect than a simple exchange of

	Energy		
	Kinetic	Potential	Total
Before interaction	0·19363	0·17510	0·36873
Centre of interaction	0·19204	0·17667	0·36871
After interaction	0·19365	0·17509	0·36874
Change during interaction	+0·00002	−0·00001	+0·00001

TABLE 1. Partition of energy at various stages of the overtaking interaction between two solitary waves

identity, for it leaves the interaction higher than the wave which comes in. The high-wave crest is now travelling faster than the incoming wave, which is in keeping with an estimate from solitary-wave theory. Similarly, the observed speed reduction of the lower wave is in qualitative agreement with a theoretical estimate. The results do seem to show that after the interaction two waves emerge which are very close to being solitary waves of translation, but that the higher wave has grown higher at the expense of the lower wave.

Figure 2 also shows the only finite feature of the interaction predicted by KdV theory – the phase shift forward of the high wave relative to where it would have been at the same time if it had not encountered a lower wave, and a similar phase shift backwards for the lower wave. The waves after interaction are travelling at different speeds, so that the value of the phase shift depends upon where it is measured. To avoid ambiguity this was done by fitting straight lines to the data on figure 2, far away from the interaction, projecting these to the interaction region, and then by measuring the horizontal displacements at the interaction centre ($t = 0$). Results are:

phase shift of the high wave 3·152 (KdV: 2·587);

phase shift of the low wave −3·792 (KdV: −4·586).

The experimental results of Weidman & Maxworthy agree with the general trend of the theoretical results, but with deviations of similar magnitude as found above.

Another item of interest is the shape of the free surface at the very rear of the two waves after interaction. Bona, Pritchard & Scott (1980) obtained numerical solutions of Peregrine's nonlinear long-wave equation and found a small trailing oscillatory wave train behind the rear wave which is not obtained from solutions of the KdV equation. The present work showed *no trace* of trailing waves, either from plots of the free surface or, more convincingly, by second differences of the point values of the surface elevation.

3.2.4. *Check on accuracy: energy partition.* The partition of energy is given in table 1. It can be seen that after 5700 time steps the total energy was conserved to high accuracy. In that time the mean depth changed by 1 part in 10^7. Considering the partition of energy before, during and after the interaction, it can be seen that changes in the system are very small indeed. Even at the centre of the interaction the energy partition is little different from the initial state: the interaction seems to be very weak.

3.2.5. *Physical discussion of solitary-wave overtaking.* In the above numerical solution of one solitary-wave overtaking interaction both major assumptions of the Korteweg–de Vries theory were found to be justified – that is, the wave motion during

interaction and at all other times was both long and low. Thus the motion was indeed weakly nonlinear, and the waves after interaction were little altered.

Examination of the experimental results of Weidman & Maxworthy show that mid-interaction heights are always considerably less than the height of the largest wave. Thus, in all cases of solitary-wave overtaking it seems that there is a nonlinear process by which fluid is transferred forward so that the front lower wave acts parasitically on the rear higher wave. The interaction time is long, so that enough fluid is moved before the main bodies of the waves coincide, and at no stage does the interaction resemble a linear superposition of the two incident waves. For small differences in the incident-wave heights this is markedly so and the two waves never coincide, while for large height differences there is apparent coalescence of the two waves but the high wave is greatly diffused by the fluid transfer. In no case does the rear wave seem to propagate through the front wave. Rather, it appears that the process involves an exchange of identity through the transference of fluid. Thus for waves which are not very different a relatively small amount has to be transferred, so that this can be done without the waves merging very much. On the other hand, for large differences in height, speed and mass, and hence in the mass to be transferred, the waves are able almost to coalesce before the redistribution is complete.

This description provides a physical explanation for the phase shift of the two crests. Figures 1 and 2 show most clearly that the fast wave crest after interaction appeared just where the slow wave crest disappeared, and *vice versa*. It does seem that the wave at the front maintained its position relative to the rear wave throughout the interaction, until it grew sufficiently for the crest to exist and subsequently to travel away. Thus if the fast wave does not have to travel through the whole interaction region, but reappears some distance forward because fluid has flowed into the front wave, the finite forward phase shift is explained. For the small wave the argument can be repeated in reverse to explain the backwards shift. While this process is easy to see in the interactions of type (*a*), where there are always two crests, it is not so obvious for interactions where a crest may temporarily disappear. Nevertheless, the fact that the phase shift is finite for all physically realizable overtaking interactions is a strong indication that the above argument holds for all.

3.3. *Interaction of different waves travelling in opposite directions*

Although the overtaking interaction has been termed 'strong' in a scattering-theory context, in the study described above it was found to be weak even though the behaviour of the interaction was essentially nonlinear. For comparison purposes the Fourier method was applied to the same two waves as in §3.2, but propagating in opposite directions – the so-called weak-interaction case. Results are given in figure 3 and in table 2, which summarizes those from the overtaking interaction as well. The interactions were of a quite different nature. In this case, as the waves came together, the crests collided and the single combined crest grew to an amplitude greater than the sum of the amplitudes of the incident waves and then subsided again as the waves emerged from each other. It was apparent that the waves had passed through each other, as shown in figure 3, rather than one wave acquiring the characteristics of the other as in the overtaking situation.

The high wave was more affected in this case – its amplitude was reduced by 0·0048 (1·5 %), $1\frac{1}{3}$ times the amount by which this wave *grew* in the overtaking case. A slightly

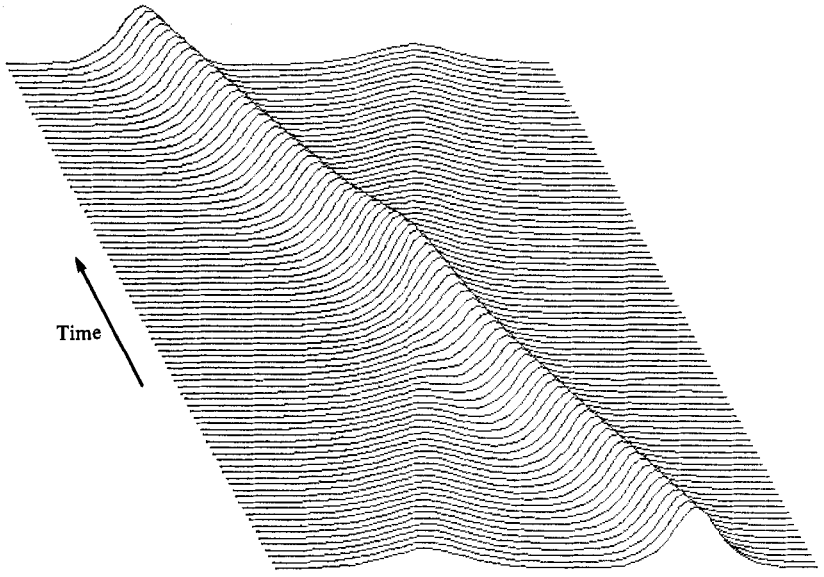

FIGURE 3. Interaction between two solitary waves of the same heights as those in figure 1, but travelling in opposite directions.

	Overtaking waves	Colliding waves
High wave		
initial crest elevation	1·3252	1·3252
final crest elevation	1·3288	1·3204
change	+0·0036	−0·0048
Low wave		
initial crest elevation	1·1035	1·1035
final crest elevation	1·1017	1·1021
change	−0·0018	−0·0014
Maximum water-surface elevation at centre of interaction	1·2096	1·4494
Relative speed of wave crests	0·1033	2·2100
Spatial phase shift: high wave	3·152	−0·446
Spatial phase shift: low wave	−3·792	−0·515
Energy proportion which is potential energy: Initial	47·49 %	47·49 %
Energy proportion which is potential energy: Centre of interaction	47·91 %	82·19 %
Energy proportion which is potential energy: Final	47·48 %	47·51 %
Energy proportion which is potential energy: Change (final − initial)	−0·01 %	+0·02 %

TABLE 2. Interaction between two solitary waves of height 0·3252 and 0·1035, comparing the two cases of (*a*) travelling in the same direction (overtaking) and (*b*) in opposite directions (colliding)

puzzling result is that the low wave was also reduced, but not as much as for the overtaking case. Energy and mass were conserved to very high accuracy during the 300 time steps used for this calculation. During the interaction the potential energy rose to as much as 82 % of the total, showing the effect of the waves colliding and the fluid being stilled as the crest rose up.

As the maximum surface elevation at the centre of the collision was 1·4494, the interaction, however brief, was highly nonlinear and in this case it is not surprising that the predictions of low-order theory – that waves pass without change except for a negative phase shift – are not so accurate.

Comparing the two sets of results in table 2, for example the change in the wave heights after interaction, it can be seen that the overtaking and colliding interactions have an effect on the waves of comparable magnitude. Hence it seems misleading to continue to describe the collision interaction as 'weak' relative to the overtaking interaction, for the brief but dramatic interaction of the former has an effect comparable to or greater than the long and low interaction of the latter. Therefore it is recommended that the previous appellations of 'weak' and 'strong' be discontinued.

In examining the colliding interaction, the third-order perturbation solution of Su & Mirie (1980) showed that each wave profile after collision was distorted because of different values of the phase shift at different points of the wave. The profile tilted backwards from the direction of propagation, but had amplitude unchanged from that before collision and travelled at the same speed. Each unsymmetric wave shed secondary waves which propagated in the opposite direction to the main wave but with diminishing amplitude due to dispersion. The theory predicts that the maximum surface elevation during collision would be 1·4509, comparing closely with the present result 1·4494. The phase shifts of the crests predicted by the theory are not as accurate. The third-order expression (55) of Su & Mirie gives post-interaction shifts of $-0{\cdot}441$ and $-0{\cdot}362$ for the low and high waves respectively, whereas the present numerical solution of the full equations gives corresponding shifts of $-0{\cdot}515$ and $-0{\cdot}446$.

The Fourier-method results also differed from those of the third-order theory in that the amplitudes after collision were diminished and the waves were travelling slightly faster. No secondary waves were discernible (see figure 3) for the interaction described above. For the case of colliding waves of equal height, discussed in §3.4, a significant secondary wave appeared only for initial wave heights greater than 0·3. Unfortunately, the long-time behaviour of the waves emerging from *one* collision cannot be examined by the method of §2, because of spatial periodicity. For higher waves than those considered here, the interaction will be even stronger. This was investigated by applying the numerical method to colliding waves of equal heights.

3.4. *Colliding waves of equal heights – solitary wave incident on a vertical wall*

3.4.1. *Computational details.* If two solitary waves of the same height propagate in opposite directions, passing through each other, then by symmetry the horizontal velocity at the centre of interaction is zero. Within the irrotational approximation then, this is the same problem as the reflection of a solitary wave by a vertical wall, and henceforth will be described in terms of the latter. To study this problem the same techniques were used as in §3.2. For a typical long wave of a given height, preliminary runs were made for various wavelengths until the interaction results were essentially independent of wavelength, when it was assumed that the wave was sufficiently close to being a solitary wave. For each wave, the speed of the crest was shown to agree very closely with the theoretical solitary-wave speed for a wave of that height, obtained from the high-order expansion for wave speed given by Fenton (1972), providing an additional check. These are shown in table 3. In the calculations $N = 32$ was used, and a typical number of 300 time steps were necessary to describe the propagation of a wave from its initial position far from the wall, its reflection, and its propagation back to that position. This required about 5 minutes of computer time.

3.4.2. *Description of the motion.* A typical reflection is shown in figure 4, for a wave of height 0·3252 of the undisturbed water depth. Initially the wave propagated without

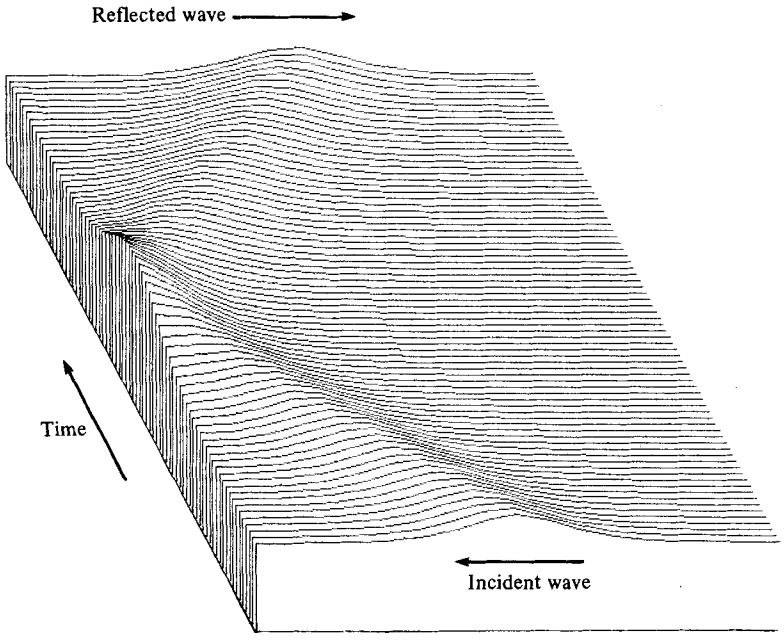

FIGURE 4. Interaction between a solitary wave of height 0·3252 and a vertical wall, or one-half of the situation of two such waves travelling in opposite directions.

change towards the wall (on the left-hand side of the figure), suggesting that it was indeed behaving like a solitary wave. The first surface profile shows an interesting feature of the computation, because the computer plot has joined points of known elevation with straight lines, so that the spacing of computational points relative to radii of curvature of the wave can be compared. The spacing is large enough that finite-difference approximation would be sorely tried, whereas the Fourier-interpolation method gave very accurate results. At the wall the water level slowly rose until it was almost as high as the crest, with the crest almost unaffected. As the intermediate trough filled, the crest 'snapped through' to the wall, in the same sense as for overtaking waves when a small transfer of fluid had a large effect on the crest. The crest at the wall then reared up to more than twice the height of the incident wave, while far from the wall the fluid was undisturbed. At its highest elevation, the crest at the wall became rather more curved. For the highest waves it became quite sharp. In this limit, the highest waves at the wall, the use of the present method becomes questionable. The sharp crest cannot be so accurately described by the Fourier series, whose accuracy depends on functions and derivatives having no discontinuities. Whereas a real wave, if sufficiently high, may show breaking (and possibly overturning) at the crest, the numerical waves were rounded by the describing trigonometric functions, and the present method could provide no breaking criterion. As will be shown below, the method still gave results agreeing closely with experiment.

After reaching the maximum height, the process was qualitatively reversed. The reflected wave was not the same as the incident wave, however, because of the nonlinear interactions. Differences will be described later; meanwhile numerical results for the problem as a whole are presented here.

ncident wave height ϵ	0·1035	0·1566	0·2134	0·2690	0·3252	0·3890	0·4554	0·5161
'hange in mean depth – accuracy check	$0{\cdot}2\times10^{-8}$	$0{\cdot}2\times10^{-7}$	$0{\cdot}1\times10^{-6}$	$0{\cdot}3\times10^{-5}$	$0{\cdot}2\times10^{-4}$	$0{\cdot}3\times10^{-4}$	$0{\cdot}2\times10^{-3}$	$0{\cdot}1\times1$
peed of crest before interaction	1·0481	1·0750	1·0974	1·1252	1·1486	1·1731	1·1970	1·2158
'heoretical solitary-wave speed	1·0502	1·0748	1·1003	1·1244	1·1480	1·1737	1·1990	1·2216
[aximum elevation of crest at wall η_m	1·2132	1·3278	1·4564	1·5866	1·7252	1·8993	2·107	2·303
[aximum force on wall F_m	0·719	0·839	0·964	1·084	1·198	1·312	1·431	1·557
[aximum moment about base M_m	0·290	0·369	0·461	0·559	0·662	0·774	0·888	1·007
)ecrease in crest elevation $\Delta\eta$	0·0006	0·0018	0·0042	0·0081	0·0138	0·0245	—	—
ncrease in crest speed Δc	$0{\cdot}002\pm1$	$0{\cdot}006\pm1$	$0{\cdot}008\pm2$	0·012	0·024	0·036	—	—
'hase lag at wall ΔT	$0{\cdot}25\pm2$	$0{\cdot}36\pm1$	$0{\cdot}40\pm1$	$0{\cdot}50\pm1$	0·61	0·73	1·12	—

TABLE 3. Results for the reflection of solitary waves of various heights by a vertical wall

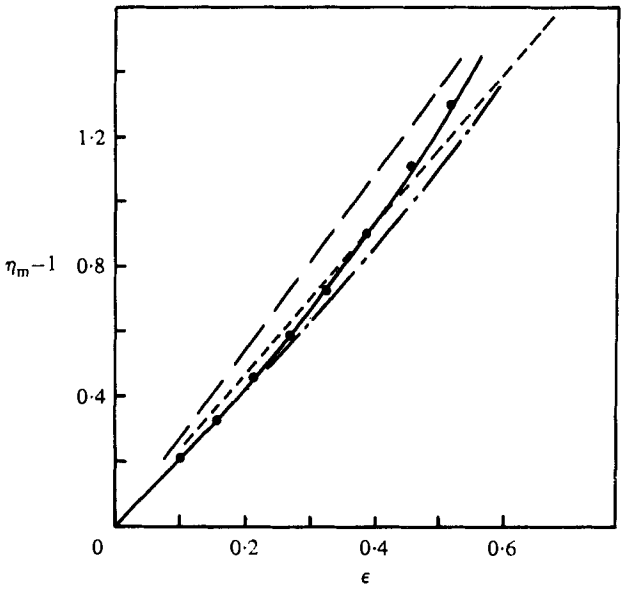

FIGURE 5. Maximum height of the crest at the wall above undisturbed depth, $\eta_m - 1$, and its variation with incident wave height ϵ. ●, Numerical results from present method; ——, third-order results of Su & Mirie (1980) and a close approximation to the numerical and experimental results reported by Chan & Street (1970); — — — —, mean of experimental results from wave-wall reflection; —— ——, wave–wave interaction, both from Maxworthy (1976). — – —, second-order theory from Byatt-Smith (1971).

3.4.3. *Results.* Table 3 contains the results for the reflection of a solitary wave by a vertical wall, which is essentially a one-parameter problem in the incident wave height. Results from this will now be considered in detail. The change in mean depth during the course of the calculations is shown for each wave height. It can be seen that the results are very accurate, except for the higher waves, whose crests became quite sharp when they struck the wall. Up to this point all solutions were very accurate,

conserving mass to four places, so that figures for maximum run-up, force and moment should be reliable. After the development of the sharp crest the solutions were less accurate, so that no results are presented for post-interaction quantities for the highest waves.

Maximum run-up at the wall. In figure 5 the maximum height of the crest above undisturbed depth, $\eta_m - 1$, is plotted against the incident wave height ϵ. Results from the present work are shown by the solid circles, which lie almost exactly on the solid line $\eta_m - 1 = 2\epsilon + \frac{1}{2}\epsilon^2 + \frac{3}{4}\epsilon^3$, the third-order result obtained by Su & Mirie (1980), which they showed agreed well with both the experimental and numerical results of Chan & Street (1970), even for the highest waves studied. It is perhaps surprising that the third-order theory describes this quantity so very accurately, while to describe the steadily progressing solitary wave accurately high-order theories are necessary. Maxworthy (1976) mentioned several experimental difficulties in obtaining results for the maximum run-up. His results are represented by the two dashed lines – the upper one having been obtained from experiments in which two oppositely directed solitary waves were generated, while the lower short-dashed line was obtained from single waves against a vertical wall.

The maximum force exerted on the wall and its moment about the base were calculated by integrating the pressure on the wall, obtained from the pressure equation at 21 equally spaced points between the bottom and the crest, using Simpson's rule. Results are given in table 3. Parabolas were fitted to these results in a least-squares sense, but requiring that the hydrostatic results for zero amplitude be recovered. These empirical results are

$$F_m = \text{force per unit length of wall}/\rho g h^2 = \tfrac{1}{2} + 2{\cdot}25\epsilon - 0{\cdot}42\epsilon^2;$$

$$M_m = \text{moment about base per unit length of wall}/\rho g h^3 = \tfrac{1}{6} + 1{\cdot}23\epsilon + 0{\cdot}80\epsilon^2.$$

As the solitary wave is the fastest, most massive, and has the greatest impulse of all waves of a given height, these results should provide convenient design criteria for vertical walls subject to wave impact.

Changes in the wave after reflection. There have been some conflicting reports concerning the shape of the wave after reflection. Byatt-Smith (1971) showed that, to second-order in wave height, the wave is unchanged. Su & Mirie (1980) obtained the third-order terms describing the interaction which contained the result that the wave *height* is unchanged after interaction, but that a third-order asymmetry about the crest is introduced, part of which subsequently appears as a dispersive trailing wave train. In their numerical solution of the full nonlinear equations Chan & Street (1970) claimed that the wave was unchanged after reflection; however, Maxworthy (1976) noted from his experiments that 'the reflected wave assumes a shape that is clearly steeper than that of the incoming wave and is ... moving slightly faster'.

A typical result from the present study is given in figure 6, which shows two wave profiles – a wave of moderate height (0·3252) before interaction, and the reflected wave when its crest was passing through the centre of the computational region. The wave was markedly different after reflection – an appreciable quantity of fluid had shifted its position, the crest was lower, the main body of the wave was wider but still almost symmetrical, and there was a finite trough behind it. As the wave propagated it was changing slowly with time; however, the present numerical method cannot be used to study the long-term evolution. The rate of change of the main wave was *very*

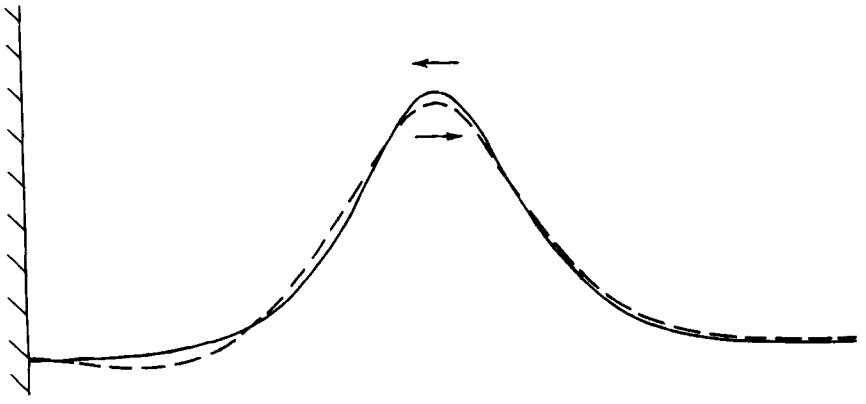

FIGURE 6. Comparison of surface profiles for an incident wave (——) of height 0·3252 of the undisturbed water depth, and the same wave (— — — —) after reflection. Vertical distortion 16:1.

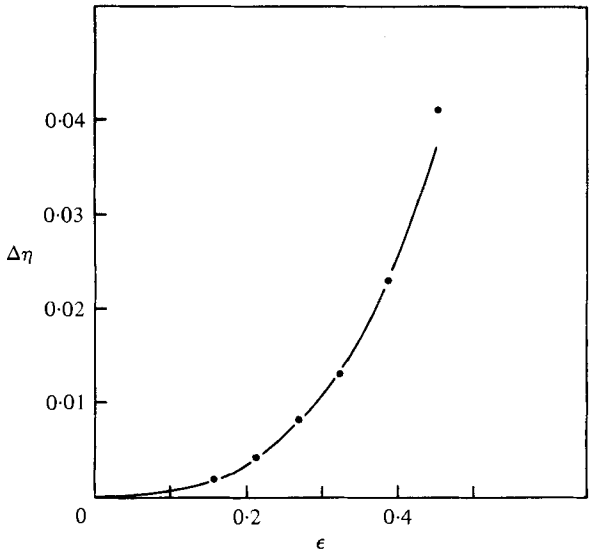

FIGURE 7. Decrease in crest elevation $\Delta\eta$ after the wave has returned to its original position. Numerical results from present work shown as solid circles. For comparison, the curve $0{\cdot}4\epsilon^3$ is shown.

small, and it propagated with sufficiently constant crest elevation, so that the decrease in crest elevation $\Delta\eta$ between incident and reflected waves could be measured and used as an indication of the change in the wave form. Values of $\Delta\eta$ for the waves studied are given in table 3, and in figure 7 are plotted against incident wave height. Assuming $\Delta\eta = a\epsilon^n$, where a and n are constants, a least-squares fit to the points gave $a = 0{\cdot}41$ and, more importantly, $n = 2{\cdot}78$, indicating strongly that changes in the wave height (and profile) are of third order. The curve $\Delta\eta = 0{\cdot}4\epsilon^3$, approximating the least-squares fit, is plotted on figure 7, and can be seen to describe the results quite closely. This would seem to throw some doubts on the results of Su & Mirie, in which no change in the crest elevation at third order is predicted.

In view of the fact that the high and fast wave in the overtaking interaction became

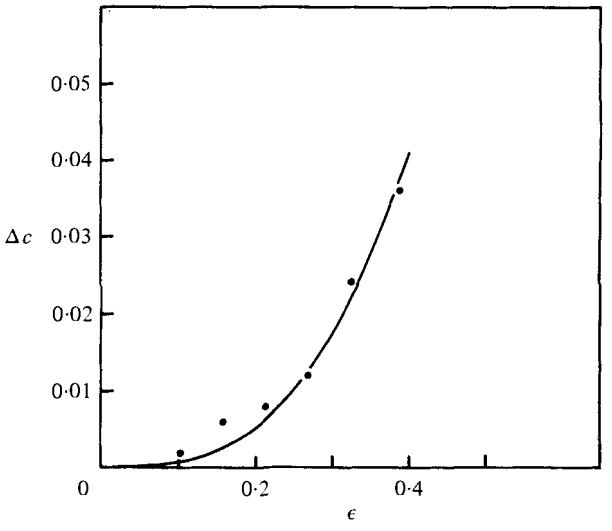

FIGURE 8. Increase in crest speed Δc after interaction. Numerical results shown as solid circles. The arbitrary curve $0{\cdot}64\epsilon^3$ is shown as ——.

higher and faster, and the lower and slower wave became even more so, the result that the waves after reflection by the wall (as shown by the results for Δc in table 3) were *faster* as well as lower seems rather surprising. Nevertheless, this was consistently obtained for all wave heights, and has been noted experimentally by Maxworthy. As all nonlinear steady-wave theories predict increasing wave speed with height for moderate heights, it seems that the reflected waves were not proper steady waves of translation (solitary waves in the long-wavelength limit). It is possible that the trailing trough (figure 6) plays a role in increasing the effective height and hence speed; however, for lower waves no local minima after reflection were found, yet they also travelled faster. Results for the increase in wave speed are plotted on figure 8. As numerical differentiation has been used to obtain the speeds from crest position data, and the actual change in speed is small, the results are less consistent than for the decrease in height, especially for lower waves. Nevertheless, a cubic curve gives a reasonable approximation, as shown on the figure. Although this increase in wave speed is small, it has important implications for the experimental measurement of phase changes, as described below.

Phase change during interaction. The change of phase of a solitary wave being reflected by a wall is shown by the idealized and exaggerated wave-crest trajectories on figure 9. A solitary-wave crest is travelling from right to left, with a wall at $x = 0$. Initially the wave does not sense the wall and travels at constant speed (at A on the diagram); however, there is a marked increase in crest speed as the body of the wave nears the wall and the region between crest and wall fills with fluid with the result that the crest 'snaps through' to the wall, arriving at B. The crest moves up the wall until it reaches a maximum, then down again until it leaves the wall at C and travels in the opposite direction. Conventionally, the phase change has been considered to be a displacement in x – the difference in location between the actual wave crest and the crest of a wave which is supposed reflected instantaneously with no change in speed so that its trajectory is AEF. Thus the phase change has been defined to be the

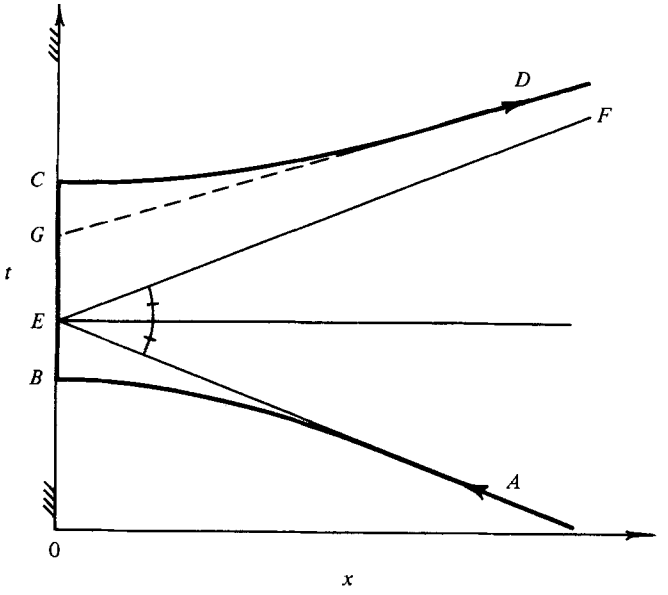

FIGURE 9. Exaggerated and schematized diagram showing crest trajectories for reflection of a solitary wave by a wall at $x = 0$. The actual wave crest follows the curves AB, BC, CD. If the wave were unaffected by the wall except for an instantaneous reflection, the crest trajectory would be AEF. The usual definition of phase lag is the horizontal distance between the lines GD and EF; however, because they are not parallel (wave speed changed by the interaction) the phase shift depends on where it is measured. In the present work, the apparent time lag EG at the wall is taken to be the phase shift.

horizontal displacement of the line GD from EF. If the slope of GD is different from the slope of EF, this displacement varies with measuring location.

The second-order theory of Oikawa & Yajima (1973) predicts that the crest travels at the same speed as before collision but is delayed at the wall so that the reflected crest trajectory is parallel to EF. Hence there is a uniform phase shift independent of measuring location, $\Delta X = (\frac{1}{3}\epsilon)^{\frac{1}{2}}$.

Su & Mirie (1980) studied such interactions to third order, finding the phase change to be a very slowly varying function of x. Immediately the reflected wave first begins to travel unaffected by the presence of the wall the phase change of the crest may be expressed as $\Delta X = (\frac{1}{3}\epsilon)^{\frac{1}{2}}(1+\frac{47}{8}\epsilon)$ (from their equation (55)). The crest is travelling faster than the hypothetical perfectly reflected wave, but with *changing* speed as the wave evolves in time; hence the phase shift is dependent on measuring location. The wave speed asymptotes to the incident wave speed, and it is only this long-time evolved wave travelling at constant speed which displays a uniform phase shift of $\Delta X = (\frac{1}{3}\epsilon)^{\frac{1}{2}}(1+\frac{7}{8}\epsilon)$, independent of measuring location.

Experimental measurements of the post-interaction phase shifts have been made (Maxworthy 1976) and show the unexplained result that the phase shift is independent of wave height, in apparent contradiction to the expression given by Su & Mirie. These experiments and the numerical results of the present work indicate that the reflected wave travels faster than the incident wave, and so the phase shift must depend on measuring location. The numerical results as plotted on figure 10 may explain the apparent experimental insensitivity to ϵ. The ordinate ΔX is the measured phase lag, plotted against incident wave height ϵ, and where the parameter x pertaining to a set

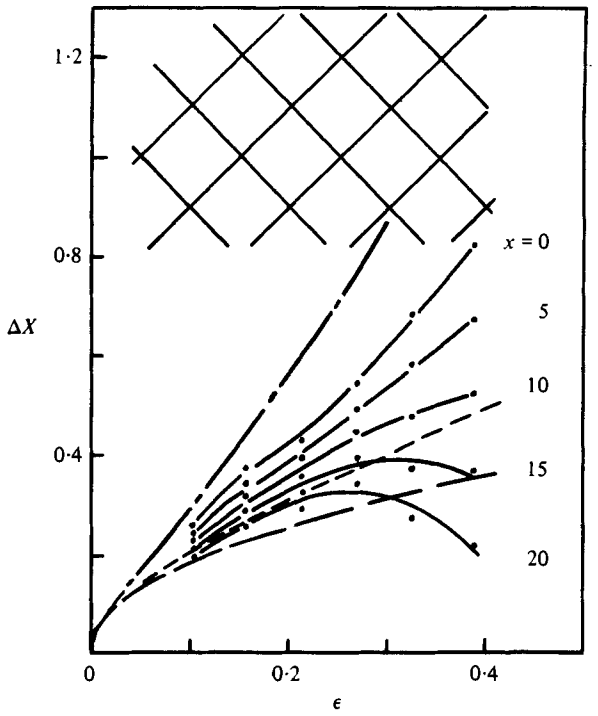

FIGURE 10. Results from the present work for spatial phase lag ΔX as a function of wave height ϵ and x, distance of measuring station from the wall. Maxworthy's results are in the hatched region, showing wide scatter about an apparent constant value of $\Delta X \simeq 1{\cdot}2$. Results from the present work are shown by points, the solid lines are curves fitted to these points, each curve corresponding to constant x. The dashed lines are from theory: ——, second-order; ——, third-order immediate post-interaction; — — —, third-order long-term.

of points and solid line is the distance from the wall at which the lag was measured. Clearly the location of the measuring station is important. For a station distant some 15–20 times the water depth, not so far in solitary-wave terms, the figure shows that the measured phase shift is relatively independent of wave height. In performing difficult physical experiments such as these, the small variation with height at, say, $x = 20$ would be swamped by experimental scatter. This may explain the observed results of Maxworthy, which are in the hatched region on figure 10, with a large scatter about an apparent constant value of $\Delta X \simeq 1{\cdot}2$. What remains to be explained is why his results are some three to four times greater than the present numerical results. It should be noted, however, that two previous presentations of the theoretical results for the case of a wave against a wall have plotted $2\Delta X$ rather than ΔX. This seems to have originated with Maxworthy (1976) in his figure 3. Comparison with his figure 2 shows that he has plotted experimental results for ΔX and theoretical results for $2\Delta X$. This was repeated by Su & Mirie (1980) in their figure 3.

These theoretical results are also plotted on figure 10, which contains the second-order theoretical result $\Delta X = (\frac{1}{3}\epsilon)^{\frac{1}{2}}$ obtained by Oikawa & Yajima (1973), and the third-order results $\Delta X = (\frac{1}{3}\epsilon)^{\frac{1}{2}}(1 + \frac{47}{8}\epsilon)$ for the immediate post-interaction stage, and $\Delta X = (\frac{1}{3}\epsilon)^{\frac{1}{2}}(1 + \frac{7}{8}\epsilon)$ for the long-term shift, both obtained by Su & Mirie (1980). It should be noted that the evolution from one to the other takes place on a very much greater length scale than the changes in the phase shift due to the different crest speed

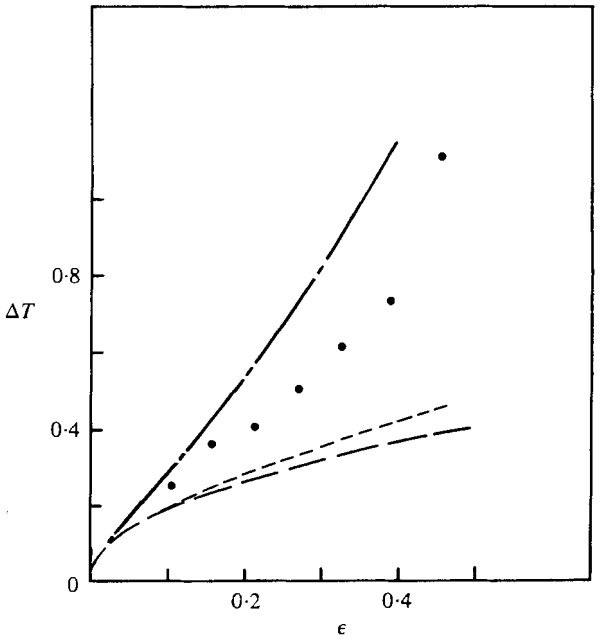

FIGURE 11. Time phase lag at the wall. ●, measured in the present work; —— ——, second-order theory; —— - ——, third-order immediate post-interaction; — — — —, third-order long-term.

as contained in the numerical results. From the figure it can be seen that these results are seeming to asymptote to the theoretical results; however, for moderate amplitudes the relatively low-order theory is not very accurate.

In view of the strong dependence of the phase lag on the measurement location, to give a unique value of phase change for a given incident wave height a definite position must be specified, for which the only unambiguous possibility is at the wall, $x = 0$. As the wave does not actually travel through the wall, rather than specifying a phase change as a *spatial* displacement it seems more reasonable to measure the phase lag in time ΔT ($=$time phase lag $\times (g/h)^{\frac{1}{2}}$ in physical terms), a quantity expressing how much longer the wave remained against the wall than if it had been instantaneously reflected. Thus, the measured phase lags given in table 3 correspond to the time displacement EG on figure 9, and are plotted on figure 11. To obtain E and G for each wave, straight lines were fitted to a number of data points in the vicinity of A and of D, using a least-squares method, and these were extrapolated to $x = 0$. As low waves are longer, so that A and D must be taken further away, the extrapolation becomes questionable in this limit even for the present idealized and accurate numerical solution. Maxworthy (1976) also reported difficulties in measuring the phase shifts accurately for small waves.

Also plotted on figure 11, with the same convention as figure 10, are the second- and third-order theoretical results, obtained from Su & Mirie's expression for ΔX, divided by the wave speed $c = 1 + \frac{1}{2}\epsilon + \ldots$, to give the phase lag ΔT: $\Delta T = (\frac{1}{3}\epsilon)^{\frac{1}{2}}(1 + \frac{43}{8}\epsilon + O(\epsilon^2))$ for the immediate post-interaction stage and $\Delta T = (\frac{1}{3}\epsilon)^{\frac{1}{2}}(1 + \frac{3}{8}\epsilon + O(\epsilon^2))$ for the long term. It can be seen that the numerical results seem to asymptote to the former for small ϵ, but that for waves of moderate height (when the numerical extrapolation

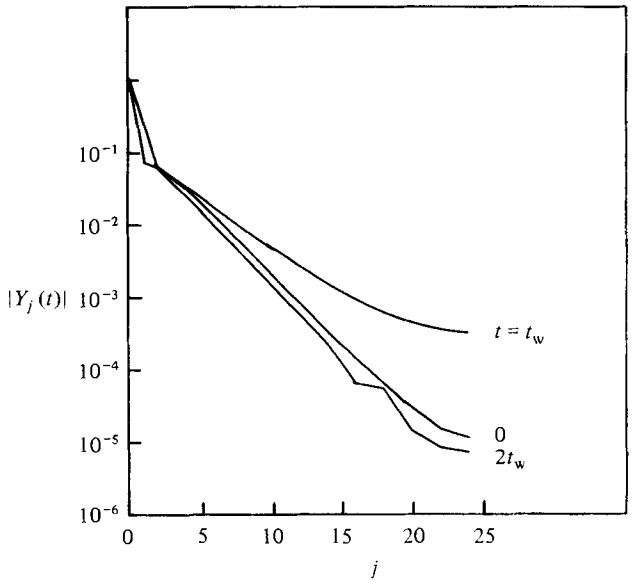

FIGURE 12. Envelopes to line spectra of the Fourier coefficients of the surface elevation, at different stages of the interaction of a solitary wave of height 0·2134 with a wall. $t = 0$ is the initial state, $t = t_w$ when the crest at the wall has reached its highest elevation, $t = 2t_w$ when the crest is back in its original position.

described above was quite accurate) the theory substantially underestimates the phase lag.

3.4.4. *The nature of the interaction.* To investigate the interaction in more detail, some more results were obtained for the case of a solitary wave of height 0·2134 being reflected by a wall, with $N = 48$. The magnitudes of the Fourier components of the surface elevation $|Y_j(t)|$ are shown by the envelopes to the line spectra, plotted on figure 12. At $t = 0$, when the wave was in the centre of the computational region and unaffected by the wall, the spectral envelope was almost a straight line on the semi-logarithmic plot, showing how the spectral components decayed almost exponentially with j. When the wave was at the wall and its crest highest ($t = t_w$), all spectral coefficients had increased substantially in order to describe the wave of greater height and sharper crest curvature. At $t = 2t_w$ when the wave had returned to its original position, but travelled in the other direction, figure 13 shows that the magnitudes of the spectral coefficients were actually *smaller* than initially, as might be expected if the interaction were such as to round off and reduce the wave crest. There was no growth of high-frequency components, the wave was still acting as a single body of water, the motion was quite coherent, and the nonlinear interaction had done nothing to break it up. This is not to imply that the wave was acting as a steady wave of translation, however, for the spectrum after the interaction was slowly changing with time, but the wave was still acting as a single entity. The rounding, smoothing nature of the nonlinear interaction in this case can be contrasted with the overtaking interaction, where the high wave grew at the expense of the low one.

Another way of characterizing the interaction is to examine the partition of energy, before, during and after the interaction, as presented in table 4. The accuracy of the calculation is shown by the almost-constant total energy. During the interaction,

Time	Kinetic energy	Potential energy	Total energy
$t = 0$ (initial conditions)	0·167252	0·149948	0·317200
$t \simeq t_w$ (at wall)	0·000313	0·316885	0·317198
$t \simeq 2t_w$ (back at initial position)	0·167027	0·150176	0·317203

TABLE 4. Energy partition at different stages of the reflection of a solitary wave of height 0·2134 from a vertical wall. As the time t_w when the crest was highest did not correspond precisely to a computational point in time, it is not possible to state that kinetic energy was or was not precisely zero when the crest was highest.

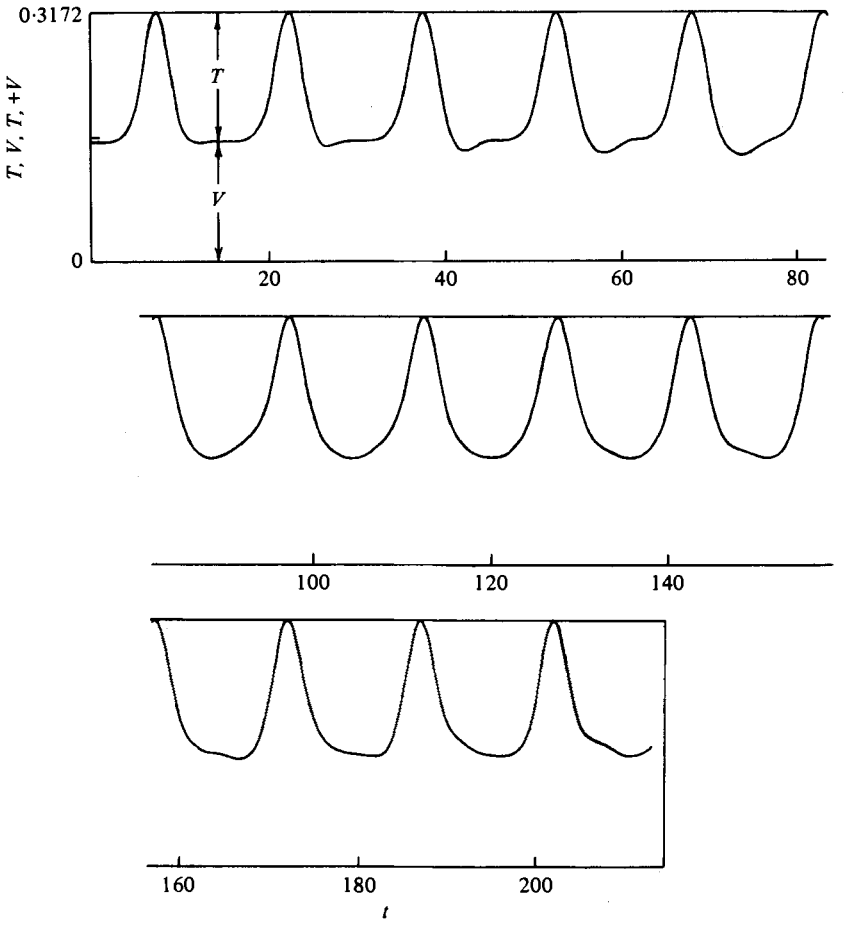

FIGURE 13. Energy partition and its variation with time for the reflection back and forth of an initial solitary wave of height 0·2134. T is kinetic energy, V is potential energy.

almost all the kinetic energy was converted into potential energy, but the collision had practically no effect on the energy partition after collision – to within 1 part in 1000 the components recovered their initial values. This was examined for higher waves too, with a similar result that even though the reflected wave was *visibly* different from the incident wave, the redistribution of mass over the whole wave was such as to give almost the same energy partition as initially.

FIGURE 14. Free-surface profile ——, initial condition of a solitary wave of translation of height 0·2134; – – – – –, instantaneous profile after nine reflections.

To investigate the behaviour of the wave during repeated interactions for a height of 0·2134 and $N = 32$, the program was run for a large number of time steps, during which time the wave was reflected repeatedly back and forth by the wall at $x = 0$, and by another wall at $x = \frac{1}{2}L$ which owed its existence to the symmetry of the problem. For these repeated interactions with the walls (or for a wave repeatedly progressing through mirror images of itself), the partition of energy is shown in figure 13. After $t = 0$, before the first interaction, the constancy of the partition shows how the wave was unaffected by the walls, then all the kinetic energy was converted into potential energy at the centre of the interaction. After this first interaction almost the same behaviour was observed, as the energy partition was unchanging while the now quasi-solitary wave travelled across the region between the walls. However, the wave had been altered so that it was changing with time. After the ninth pass of the wave the partition was varying continually, and so symmetrically about the centre of the region that a periodic standing-wave motion was suggested. However, details of the motion did not bear this out. After that pass the partition seemed to be steadily evolving back to that of a solitary 'mound' – see time 180 on figure 13 – where the partition changed little while the wave was away from the walls. At all stages, however, the wave form was slowly changing as it propagated, and the partitition of energy continued to change from pass to pass. No steady-state periodic motion was observed, no substantial recurrence phenomena were observed. The maximum crest elevation of the wave was further degraded after each interaction. At no time was there visible evidence of high harmonics: the wave continued to act as a whole, albeit a slowly and continuously changing whole. While no marked phenomena were observed, this *coherence* of the motion was interesting – the entire motion did seem to be bound to the main wave. As an illustration, figure 14 shows the wave profile initially, and at the centre of the tenth pass, at which time the wave momentarily was quite symmetrical.

The authors would like to thank their colleagues, and in particular P. J. Blenner-hassett and W. D. McKee, for many helpful discussions and suggestions during the course of this work. Partial support was provided by the Faculty of Science, University of N.S.W., and by the Australian Research Grants Council.

Appendix. Waves over uneven topography

Consider a layer of fluid whose motion is irrotational and two-dimensional over an irregular moving bottom so that the free surface is $y = \eta(x,t)$, but the bottom is defined by $y = h(x,t)$ instead of $y = 0$ as above. The boundary condition that the velocity normal to the bed is zero may be written

$$h_t + \phi_x h_x - \phi_y = 0 \quad \text{on} \quad y = h(x,t), \tag{A 1}$$

where the function $h(x,t)$ is known. For this more general case, (A 1) replaces (4); otherwise all other equations governing the motion ((1)–(3)) are the same. It is assumed that all variables have been non-dimensionalized with respect to some length scale, typically a mean depth as in §2.1, and gravitational acceleration g.

A series representation for ϕ satisfying only the field equation (1) is

$$\phi(x,y,t) = \frac{1}{N}\sum_{j=-\frac{1}{2}N}^{\frac{1}{2}N}(A_j(t)\cosh jky + B_j(t)\sinh jky)\,e^{-ijkx}, \tag{A 2}$$

where a factor of $\frac{1}{2}$ multiplies the contributions at $j = \pm\frac{1}{2}N$. As ϕ is real,

$$A_{-j} = A_j^*, \quad B_{-j} = B_j^*. \tag{A 3}$$

For notational purposes (A 2) is used here rather than the form obtained when (A 3) is used to express ϕ explicitly as a real quantity. (A 2) is differentiated to give

$$\frac{\partial\phi}{\partial x}(x,y,t) = \frac{-ik}{N}\sum_j j(A_j(t)\cosh jky + B_j(t)\sinh jky)\,e^{-ijkx}, \tag{A 4}$$

$$\frac{\partial\phi}{\partial y}(x,y,t) = \frac{k}{N}\sum_j j(A_j(t)\sinh jky + B_j(t)\cosh jky)\,e^{-ijkx}, \tag{A 5}$$

$$\frac{\partial\phi}{\partial t}(x,y,t) = \frac{1}{N}\sum_j\left(\frac{\partial A_j(t)}{\partial t}\cosh jky + \frac{\partial B_j(t)}{\partial t}\sinh jky\right)e^{-ijkx}. \tag{A 6}$$

If all the surface elevations and Fourier coefficients are known at successive times $t-\Delta t$ and t, then the surface elevations at $t+\Delta t$ are simply obtained from the centred-difference approximation to (3):

$$\eta(x_m, t+\Delta t) = \eta(x_m, t-\Delta t) - 2\Delta t\{\phi_y(x_m,\eta_m,t) - \phi_x(x_m,\eta_m,t)\,\eta_x(x_m,\eta_m,t)\} + O((\Delta t)^3), \tag{A 7}$$

where the η_x are obtained from (8). To advance the Fourier coefficients in time is rather more complicated. Surface values of ϕ_t at time t may be obtained from the pressure equation (2) so that $\phi_t(x_m,\eta_m,t)$ are known for $m = -\frac{1}{2}N, \ldots, \frac{1}{2}N-1$. Replacing the time derivatives in (A 6) by the finite-difference approximations gives

$$\sum_j\{(A_j(t+\Delta t) - A_j(t-\Delta t))\cosh jk\eta(x_m,t) + (B_j(t+\Delta t) - B_j(t-\Delta t))\sinh jk\eta(x_m,t)\}\,e^{-ijkx_m} - 2N\Delta t\,\phi_t(x_m,\eta_m,t) = O((\Delta t)^3)$$
$$(m = -\tfrac{1}{2}N, \ldots, \tfrac{1}{2}N-1). \tag{A 8}$$

Using (A 3) and the approximation that the right-hand side is zero gives a set of N linear equations in the $2N$ real unknowns from

$$\{A_0(t+\Delta t), A_j(t+\Delta t), B_j(t+\Delta t), j = 1,\ldots,\tfrac{1}{2}N\},$$

where $\mathscr{I}(A_0) = 0$ and it is assumed that $\mathscr{I}\{A_{\frac{1}{2}N}\} = 0$.

The remaining N equations are obtained by satisfying the kinematic boundary condition on the bottom (A 1) at time $t+\Delta t$, into which (A 4) and (A 5) are substituted:

$$\frac{k}{N}\sum_j j\{A_j(t+\Delta t)\,[ih_x(x_m,t+\Delta t)\cosh jkh(x_m,t+\Delta t) + \sinh jkh(x_m,t+\Delta t)] + B_j(t+\Delta t) \times [ih_x(x_m,t+\Delta t)\sinh jkh(x_m,t+\Delta t) + \cosh jkh(x_m,t+\Delta t)]\}\,e^{-ijkx_m} - h_t(x_m,t+\Delta t) = 0$$
$$(m = -\tfrac{1}{2}N, \ldots, \tfrac{1}{2}N-1). \tag{A 9}$$

The relations (A 3) are again used to ensure that these equations are real. At each time step, $2N$ linear equations (A 8) and (A 9) in $2N$ unknowns must be solved, to advance

the solution. When $\eta(x_m, t+\Delta t)$, for all m, and $A_j(t+\Delta t)$ and $B_j(t+\Delta t)$ are all known, the procedure can be repeated at the next time step, and so on.

In this case, the implied periodicity of the problem may present more of a limitation than in situations where the bed is only horizontal. Nevertheless there are many problems, such as the scattering of a solitary wave by a single hump, which may be quite accurately simulated by this method.

REFERENCES

ABE, K. & INOUE, O. 1980 Fourier expansion solution of the Korteweg–de Vries equation. *J. Comp. Phys.* **34**, 202–210.

BONA, J. L., PRITCHARD, W. G. & SCOTT, L. R. 1980 Solitary wave interaction. *Phys. Fluids* **23**, 438–441.

BRENNEN, C. 1971 Some numerical solutions of unsteady free surface wave problems using the Lagrangian description of the flow. In *Proc. 2nd Int. Conf. Numerical Methods in Fluid Dynamics, Berkeley*, 1970 (ed. M. Holt), Lecture Notes in Physics, vol. 8, pp. 403–409. Springer.

BYATT-SMITH, J. G. B. 1971 An integral equation for unsteady surface waves and a comment on the Boussinesq equation. *J. Fluid Mech.* **49**, 625–633.

CHAN, R. K. C. & STREET, R. L. 1970 A computer study of finite-amplitude water waves. *J. Comp. Phys.* **6**, 68–94.

FENTON, J. D. 1972 A ninth-order solution for the solitary wave. *J. Fluid Mech.* **53**, 257–271.

FENTON, J. D. & MILLS, D. A. 1977 Shoaling waves: numerical solution of exact equations. In *Proc. I.U.T.A.M. Symp. Waves on water of variable depth, Canberra* (ed. D. G. Provis & R. Radok), Lecture Notes in Physics, vol. 64, pp. 94–101. Springer.

FORNBERG, B. & WHITHAM, G. B. 1978 A numerical and theoretical study of certain nonlinear wave behaviour. *Phil. Trans. R. Soc. Lond.* A **289**, 373–404.

HIROTA, R. 1971 Exact solution of the Korteweg–de Vries equation for multiple collisions of solitons. *Phys. Rev. Lett.* **27**, 1192–1194.

LONGUET-HIGGINS, M. S. & COKELET, E. D. 1976 The deformation of steep surface waves on water I. A numerical method of computation. *Proc. R. Soc. Lond.* A **350**, 1–26.

MAXWORTHY, T. 1976 Experiments on collisions between solitary waves. *J. Fluid Mech.* **76**, 177–185.

MULTER, R. H. 1973 Exact nonlinear model of wave generator. *J. Hyd. Div. A.S.C.E.* **99**, 31–46.

OIKAWA, M. & YAJIMA, N. 1973 Interactions of solitary waves – a perturbation approach to nonlinear systems. *J. Phys. Soc. Japan* **34**, 1093–1099.

ORSZAG, S. A. 1971 Numerical simulation of incompressible flows within simple boundaries: accuracy. *J. Fluid Mech.* **49**, 75–112.

RIENECKER, M. M. & FENTON, J. D. 1981 A Fourier approximation method for steady water waves. *J. Fluid Mech.* **104**, 119–137.

SU, C. H. & MIRIE, R. M. 1980 On head-on collisions between two solitary waves. *J. Fluid Mech.* **98**, 509–525.

WEIDMAN, P. D. & MAXWORTHY, T. 1978 Experiments on strong interactions between solitary waves. *J. Fluid Mech.* **85**, 417–431.

WHITNEY, A. K. 1971 The numerical solution of unsteady free surface flows by conformal mapping. In *Proc. 2nd Int. Conf. Numerical Methods in Fluid Dynamics, Berkeley*, 1970 (ed. M. Holt), Lecture Notes in Physics, vol. 8, pp. 458–462. Springer.